Extended Data Fig. 1

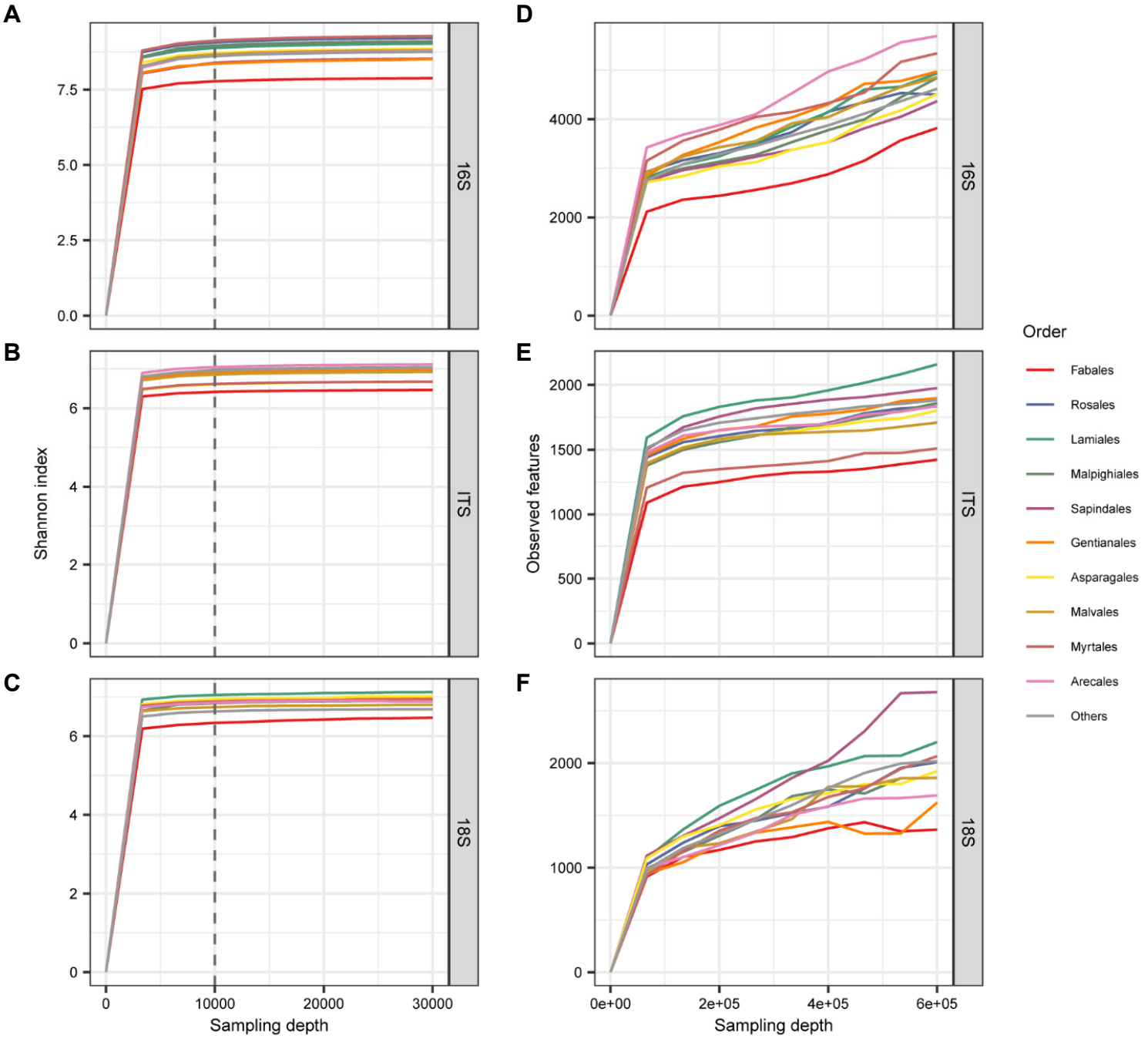

Extended Data Fig. 1. Diversity saturation of rhizosphere bacteria, fungi, and protists, related to Fig. 1A

(A–C) Shannon diversity of observed ASVs for bacterial (16S *rRNA* gene; **A**), fungal (ITS; **B**), and protistan (18S *rRNA* gene; **C**) communities at increasing sequencing depths across plant lineages (curves colored by plant order). Subsampling at 10,000 sequences per sample captured near-complete taxonomic diversity across all groups, confirming sequencing depth adequacy.

(D–F) Rarefaction analysis of ASV richness for bacterial (16S *rRNA* gene; **D**), fungal (ITS; **E**), and protistan (18S *rRNA* gene; **F**) communities at increasing sequencing depths across plant lineages. Despite sequencing depths exceeding 600,000 sequences per sample, rarefaction curves failed to plateau, indicating persistent detection of low-abundance taxa within the wild plant rhizosphere.

Extended Data Fig. 2

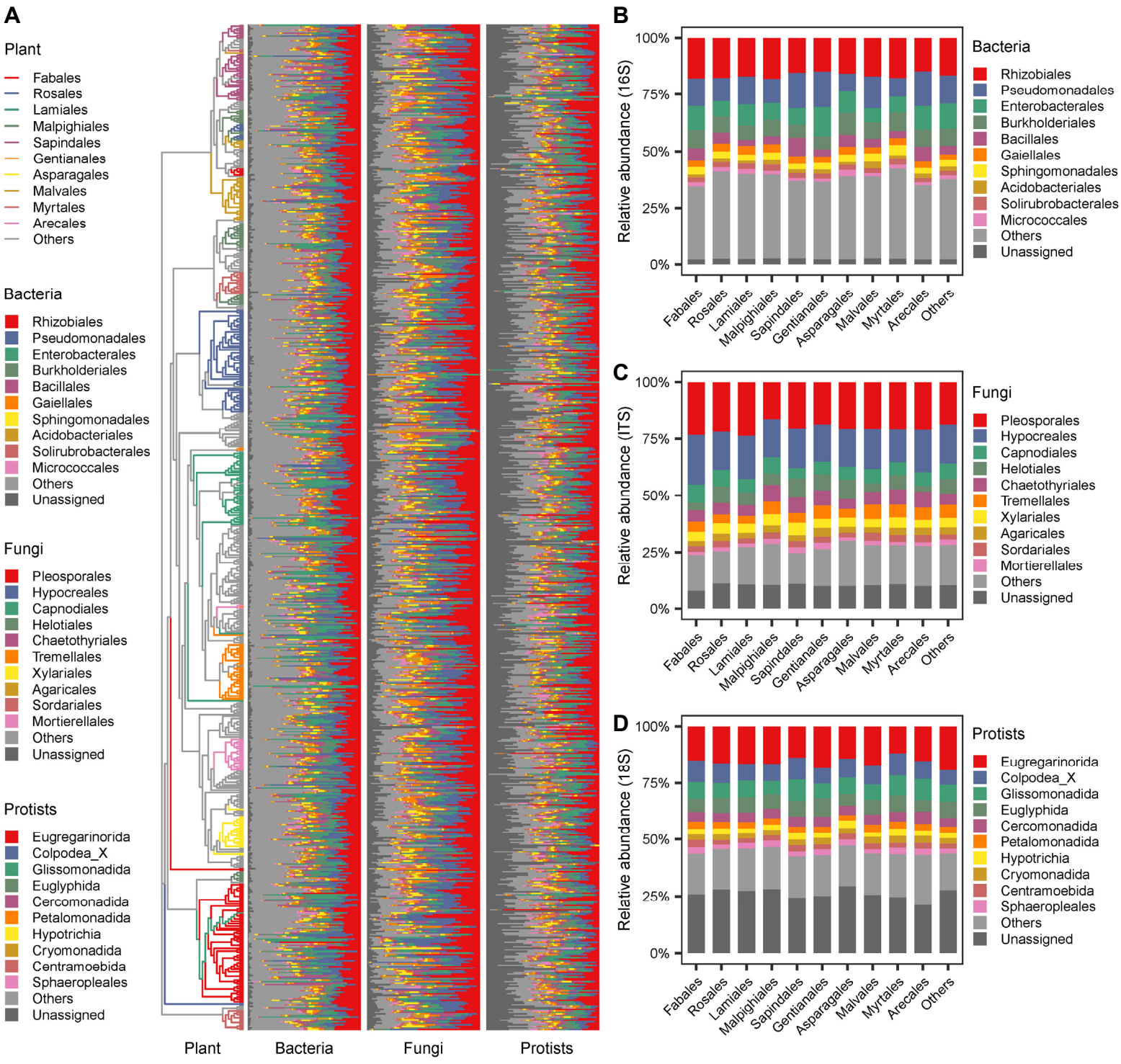

Extended Data Fig. 2. Order-level taxonomic composition and plant-phylogeny associations of rhizosphere microbiota, related to Fig. 1A

(**A**) Phylogenetic tree of vascular plant orders (e.g., Fabales, Rosales, Malvales) showing host lineage distribution. (**B–D**) Stacked bar plots depicting relative abundance of bacterial (B), fungal (C), and protistan (D) orders across plant hosts.

Extended Data Fig. 3

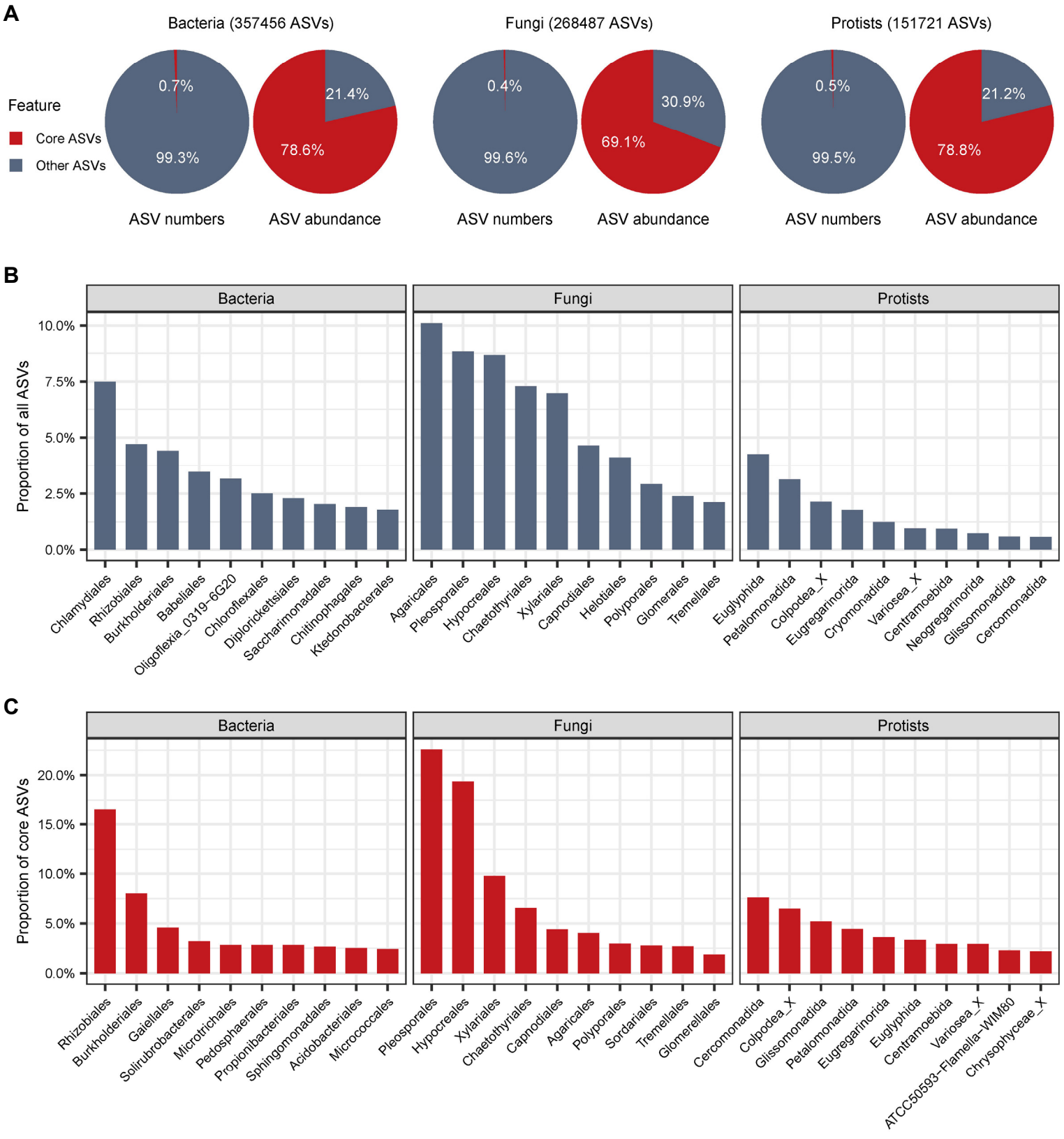

Extended Data Fig. 3. Richness-abundance decoupling and core taxa dominance in rhizosphere microbiota, related to Fig. 1A

(A) Proportional contribution of core (present in >20% of samples; red) and non-core (grey) ASVs to total taxonomic richness (ASV counts, left pie) and community relative abundance (right pie). Core ASVs constituted minimal richness fractions (bacteria: 0.7%; fungi: 0.4%; protists: 0.5%) but dominated abundance (bacteria: 78.6%; fungi: 69.1%; protists: 78.8%).

(B) Relative ASV richness across bacterial, fungal, and protistan orders. Bacterial ASVs were dominated by *Chlamydiales* (7.49%), fungal ASVs by *Agaricales* (10.10%), and protistan ASVs by *Euglyphida* (4.26%).

(C) Taxonomic composition of **core ASVs**, revealing distinct enrichment in *Rhizobiales* (bacteria), *Pleosporales* (fungi), and *Cercomonadida* (protists).

Extended Data Fig. 4

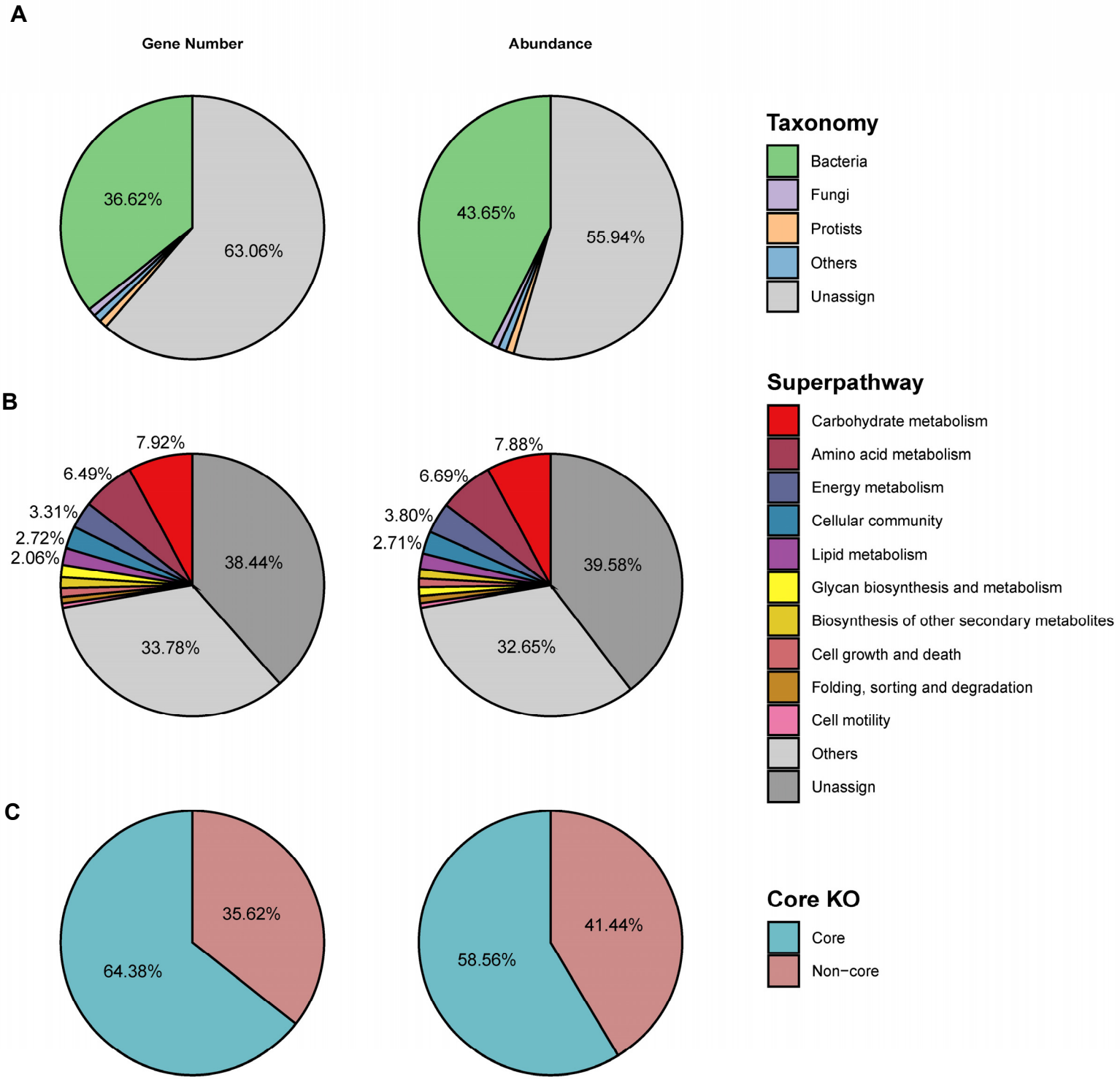

Extended Data Fig. 4. Taxonomic and functional landscape of rhizosphere metagenomes reveals uncharted diversity and core metabolic conservation, related to Fig. 1B

(A) Gene catalog taxonomy: Bacterial genes dominated (36.62% of 479.69M nonredundant genes; green), while fungal (0.0123%; purple) and protistan (0.00287%; orange) genes were rare. Critically, 63.06% of genes (gray) were taxonomically unclassified.

(B) Functional annotation: KEGG superpathway distribution of all genes. Carbohydrate metabolism (red), amino acid metabolism (dark purple), and energy metabolism (teal) constituted dominant conserved functions across plant orders. Notably, 38.44% of genes lacked KEGG annotation (39.58% abundance; gray), indicating novel functions.

(C) Core functional genes: Defined as KEGG Orthologs (KOs) present in >50% of samples. Core KOs constituted 58.56% of total functional abundance (light blue) yet represented 64.38% of KO richness, confirming functional redundancy.

Extended Data Fig. 5

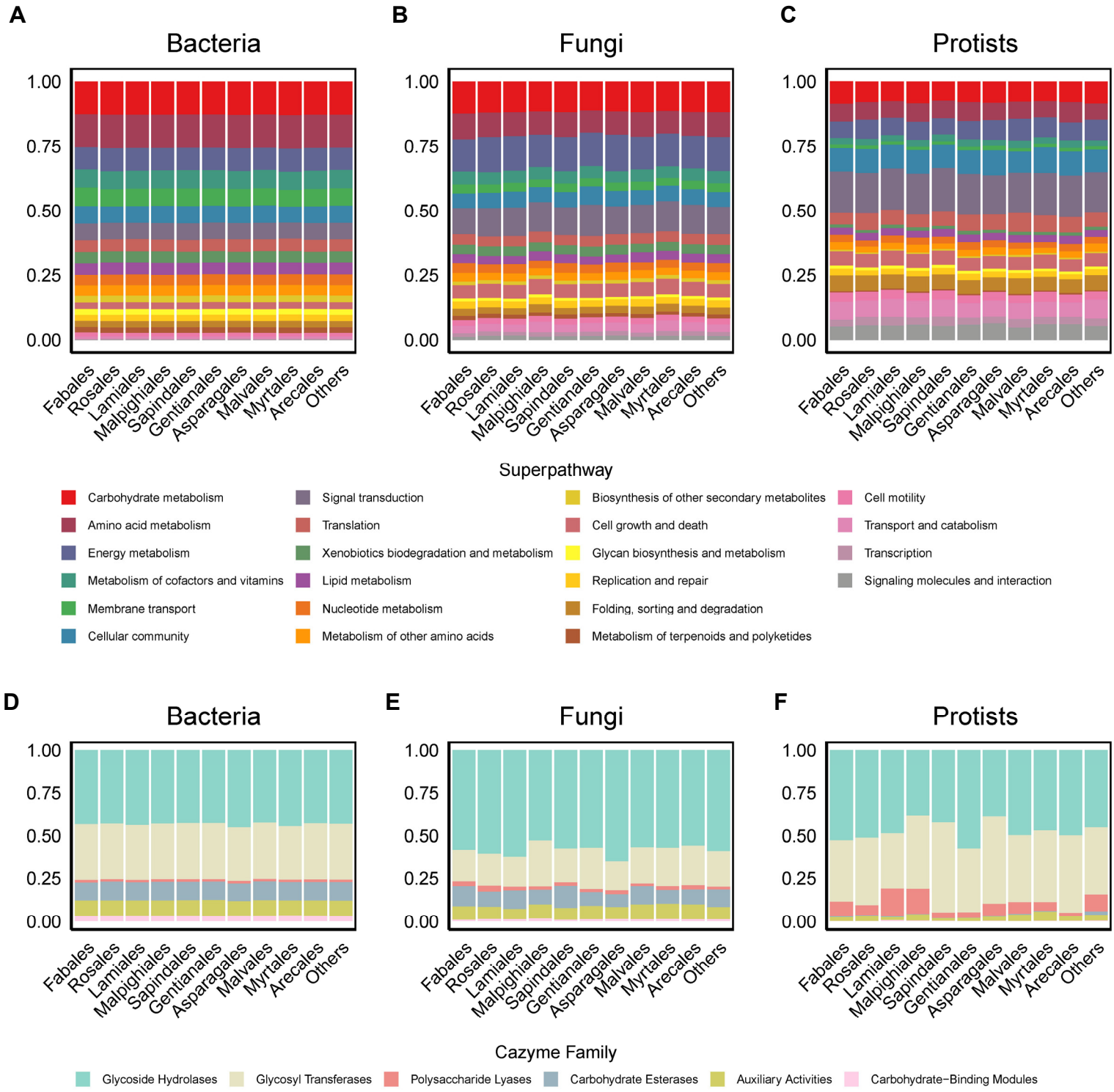

Extended Data Fig. 5. Conserved functional profiles across plant lineages but kingdom-specific metabolic specialization in rhizosphere microbiota, related to Fig. 1B

(**A–C**) KEGG superpathway distributions for bacteria (A), fungi (B), and protists (C) across vascular plant orders. Bacteria: Dominated carbohydrate metabolism, amino acid metabolism, and membrane transport; Fungi/Protists: Enriched in signal transduction, cell growth/death, and transport/catabolism.

(**D–F**) CAZy enzyme family abundances for bacteria (D), fungi (E), and protists (F): Fungi: Pronounced glycoside hydrolases (GHs) for cellulose/xylan hydrolysis; Protists: Elevated glycosyl transferases (GTs) and polysaccharide lyases (PLs); Bacteria: Minimal GHs but enriched carbohydrate-binding modules (CBMs).

Extended Data Fig. 6

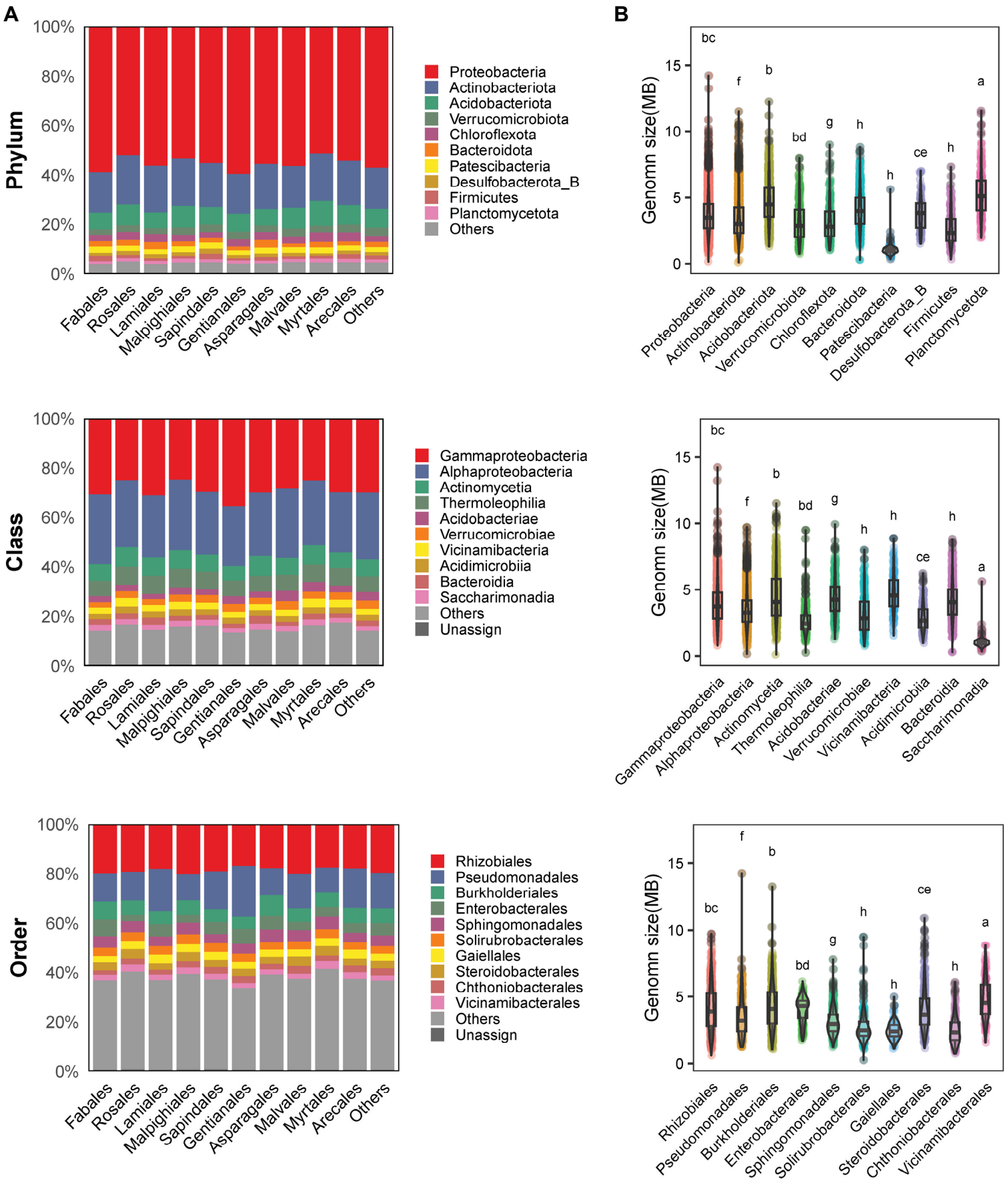

Extended Data Fig. 6. Taxonomic composition and genome size diversification of reconstructed SGBs reveals unexplored diversity and phylum-specific evolutionary niches, related to Fig. 1C

(**A**) Taxonomic composition: Stacked bar charts show relative abundance of SGBs at five taxonomic ranks (phylum to order).

(**B**) Genome size distribution: Violin plots for top 10 taxa at each rank reveal phylum-specific adaptations: Planctomycetota: Large (>7 Mb), size-constrained genomes (low plasticity). Proteobacteria: Extreme genome plasticity (1–10 Mb; minimal to giant genomes). Verrucomicrobia/Bacteroidetes and Firmicutes/Actinobacteriota: Statistically distinct, conserved size niches.

Extended Data Fig. 7

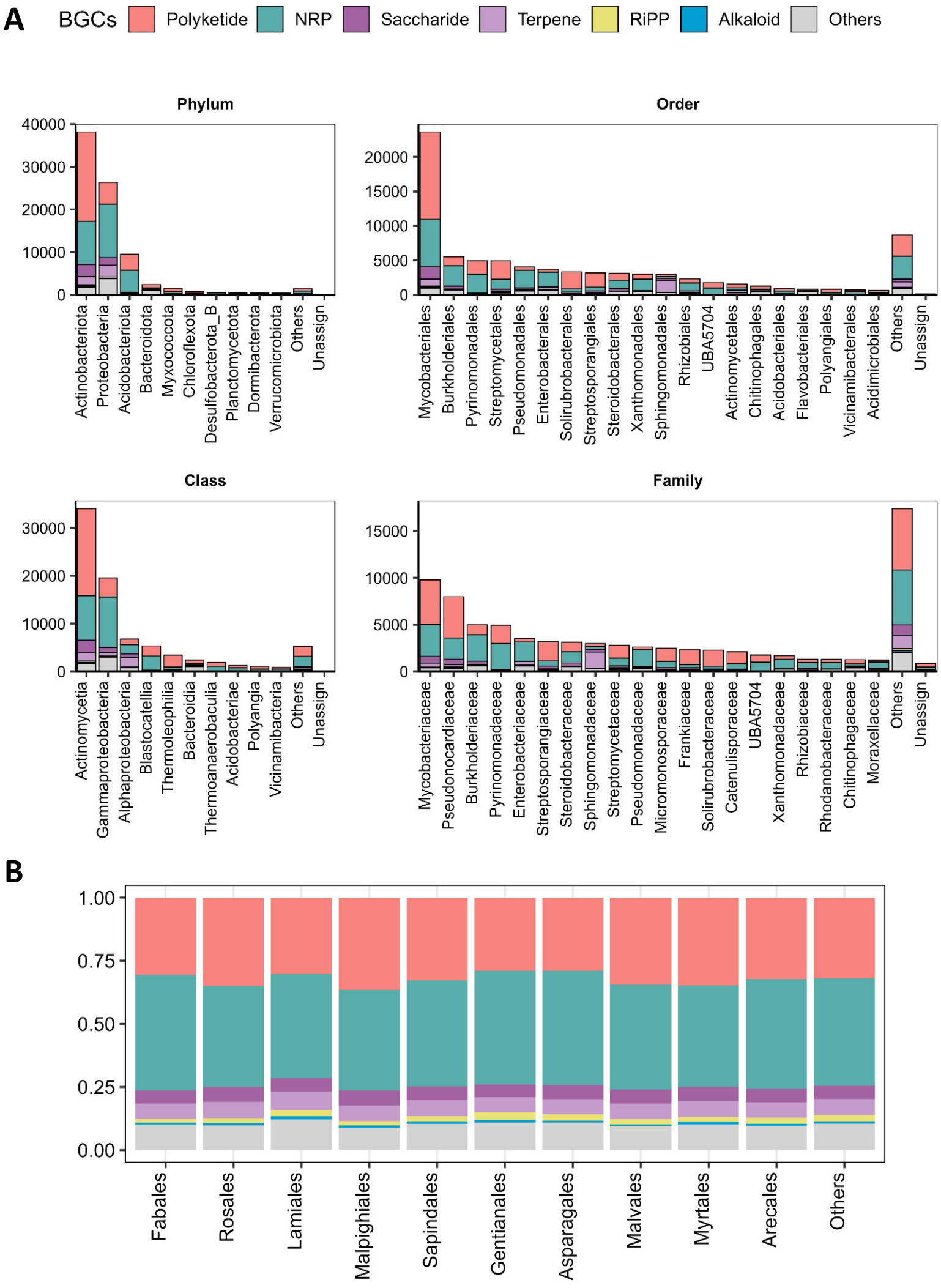

Extended Data Fig. 7. Taxonomic associations and plant-lineage conservation of biosynthetic gene clusters (BGCs) in rhizosphere microbiota, related to Supplementary Information Table 5B

(**A**) Taxonomic distribution of BGC classes across microbial ranks (phylum, order, class, family). Stacked bars illustrate dominant associations: Polyketide BGCs (red): Enriched in *Mycobacteriales*, *Streptomycetales*, *Solirubrobacterales*, *Streptosporangiales*; Nonribosomal peptide (NRP) BGCs (teal): Prevalent in *Burkholderiales*, *Pyrinomonadales*, *Pseudomonadales*, *Enterobacterales;* Terpene BGCs (light purple): Dominant in *Sphingomonadales*; Saccharide BGCs (pink): Highest in *Mycobacteriales.*

(**B**) Conservation of BGC-type proportions across vascular plant lineages (Fabales to Arecales). Bar plots reveal consistent distributions of core BGC classes (*Polyketide*, *NRP*, *Saccharide*, *Terpene*) despite taxonomic variation in host-associated microbiota.

Extended Data Fig. 8

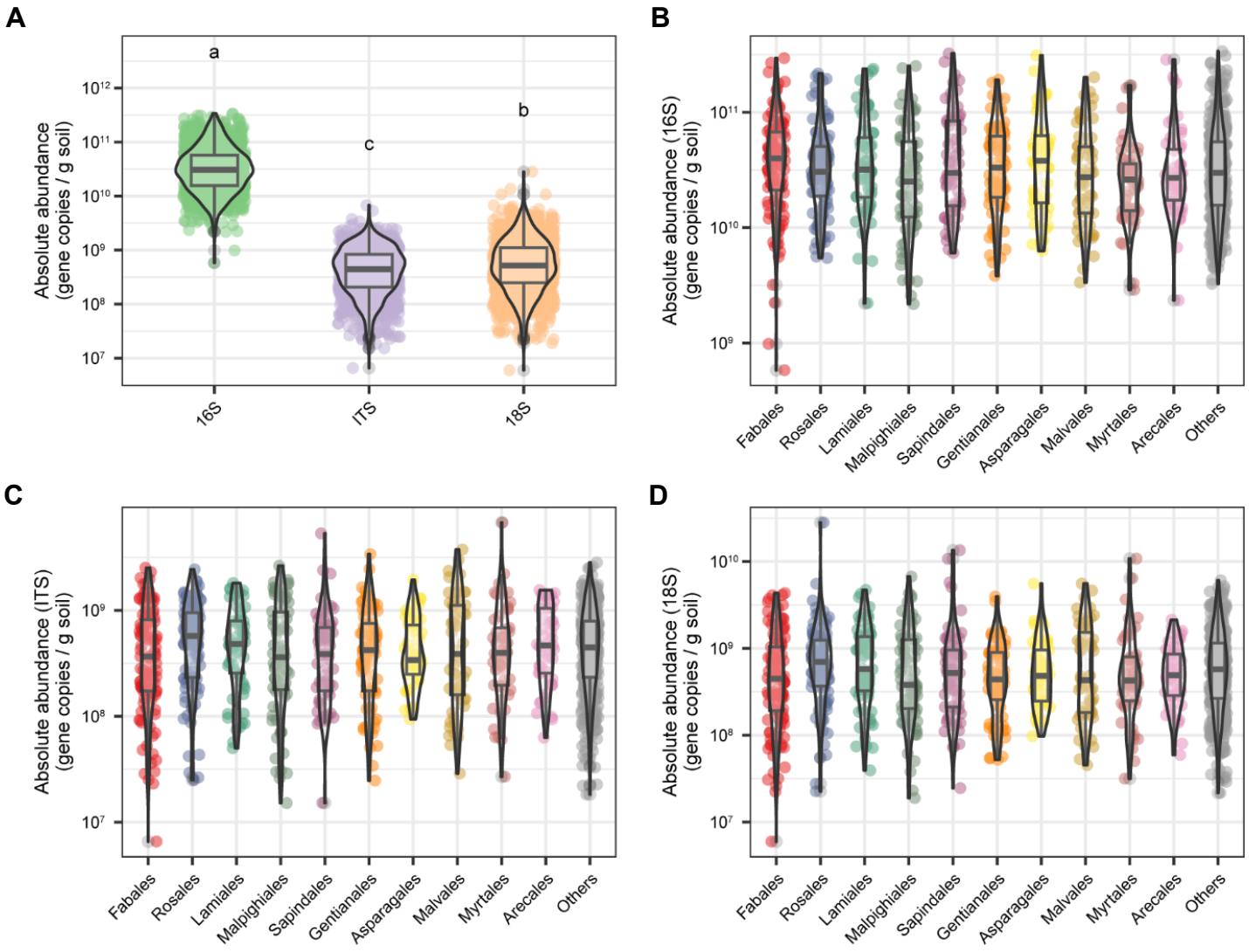

Extended Data Fig. 8. Quantitative microbiome profiling reveals domain-specific abundance scaling and plant-lineage conservation of microbial loads, related to Fig. 2

(**A**) Domain-specific absolute abundances: Boxplots of log10-transformed microbial loads per gram soil show orders-of-magnitude differences between kingdoms: Bacteria: (4.34 ± 3.82) × 10^{10} 16S *rRNA* gene copies (green); Fungi: (9.46 ± 1.27) × 10^{8} ITS copies (purple); Protists: (1.39 ± 2.35) × 10^{9} 18S gene copies (orange).

(**B–D**) Plant-lineage conservation: Microbial loads for bacteria (B), fungi (C), and protists (D) show no significant variation across vascular plant orders (Fabales to Arecales; $p > 0.05$).

Extended Data Fig. 9

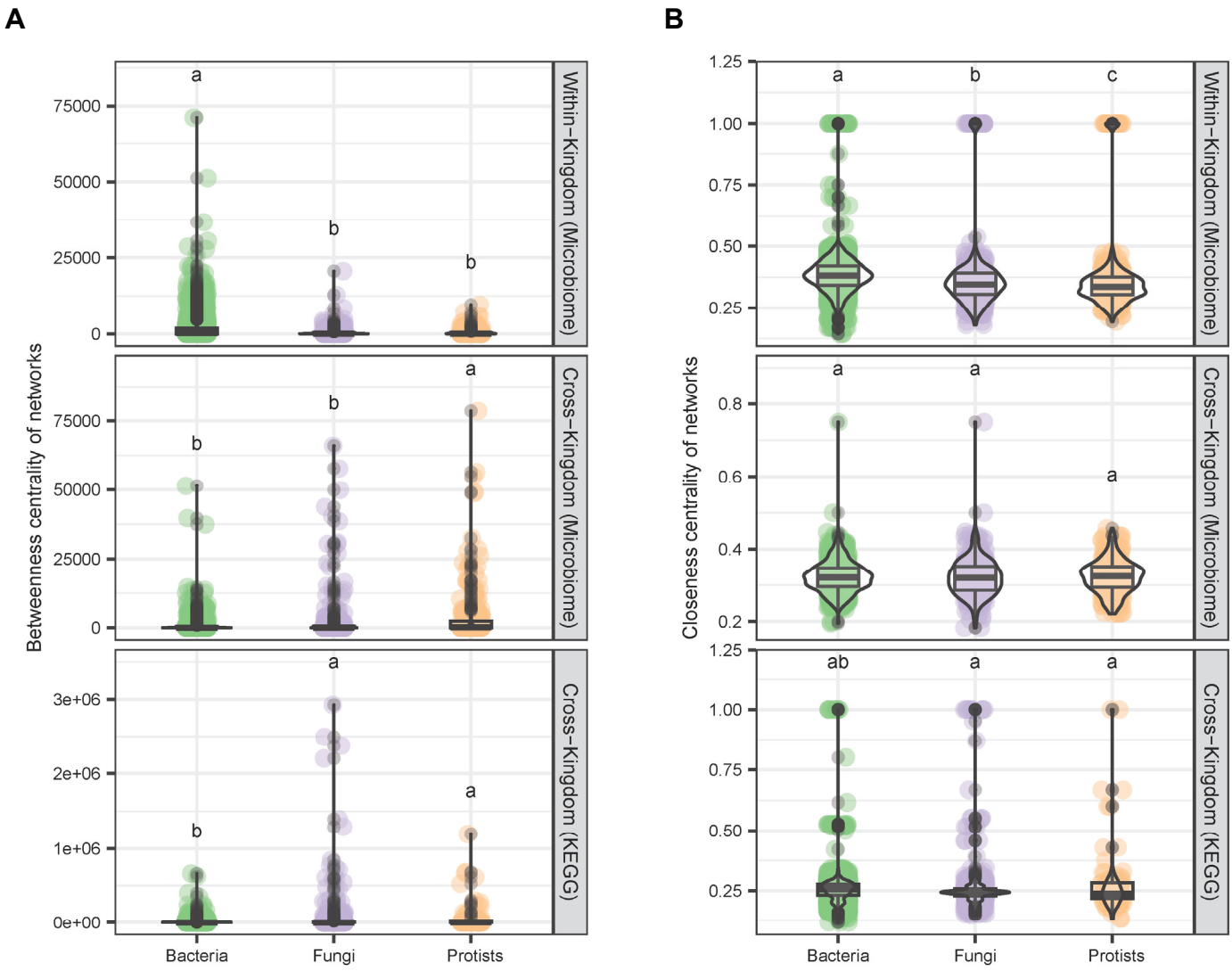

Extended Data Fig. 9. Centrality metrics reveal bacterial dominance in rhizosphere interaction networks, related to Fig. 3

Boxplots comparing betweenness centrality (**A**) and closeness centrality (**B**) of bacterial, fungal, and protistan ASVs/KOs in within-kingdom (amplicons), cross-kingdom (amplicons) and cross-kingdom (metagenome) association networks. Statistical significance denoted by lowercase letters (a-c).

Extended Data Fig. 10

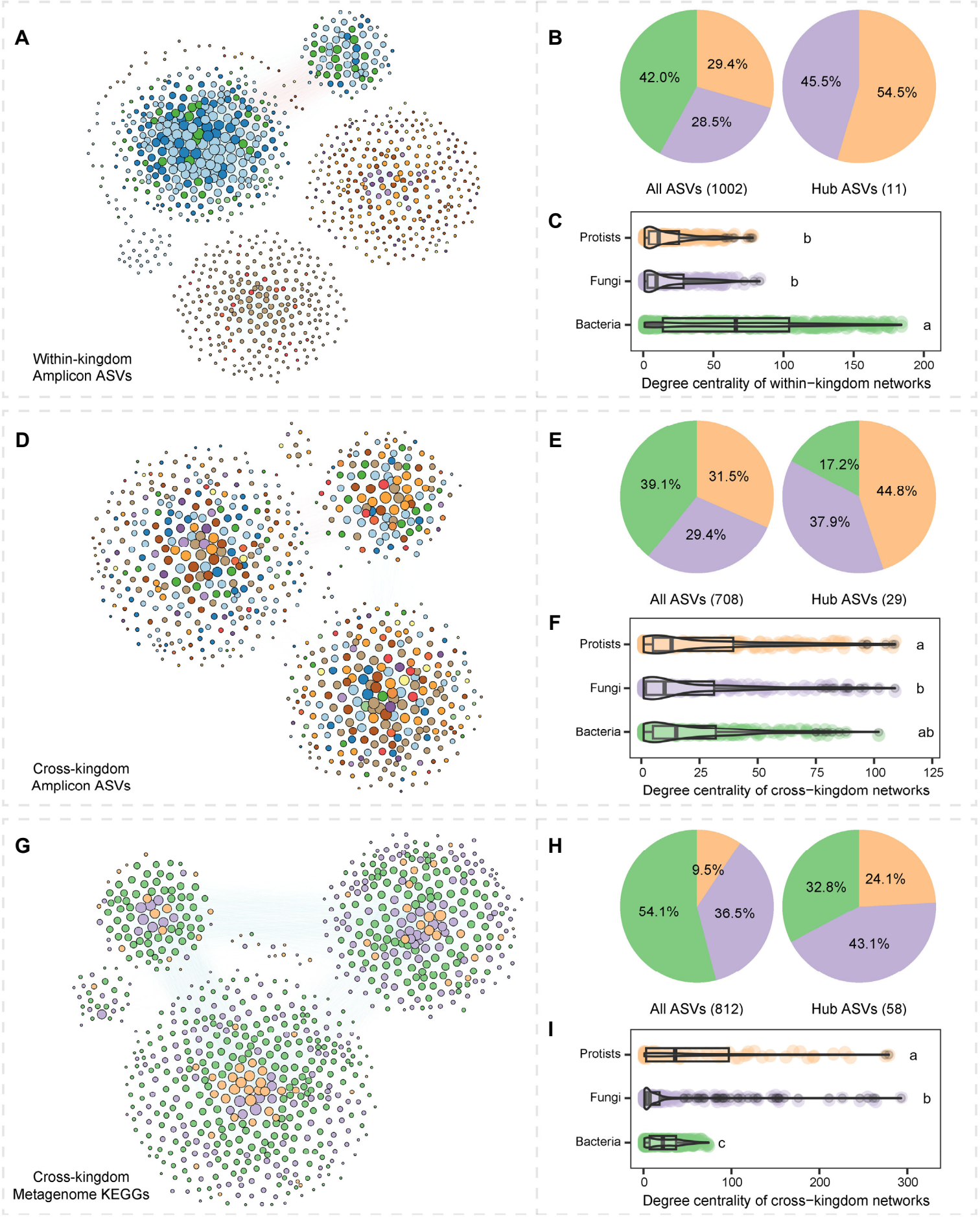

Extended Data Fig. 10. Validation of protistan and fungal keystone dominance in rarefied networks confirms intrinsic interkingdom roles, related to Fig. 3.

(A) Rarefied Intrakingdom taxonomic networks (equal ASV representation) with top 500 core ASVs per kingdom. **(B)** Proportional representation of all and hub ASVs. **(C)** Degree centrality distributions by kingdom.

(D) Rarefied interkingdom taxonomic networks (equal ASV representation) with top 500 core ASVs per kingdom. **(E)** Proportional representation of all and hub ASVs. **(F)** Degree centrality distributions by kingdom.

(**G)** Rarefied interkingdom functional networks (equal KO representation) with top 500 core KOs per kingdom. **(H)** Proportional representation of all and hub KOs. **(I)** Degree centrality distributions by kingdom.

Extended Data Fig. 11

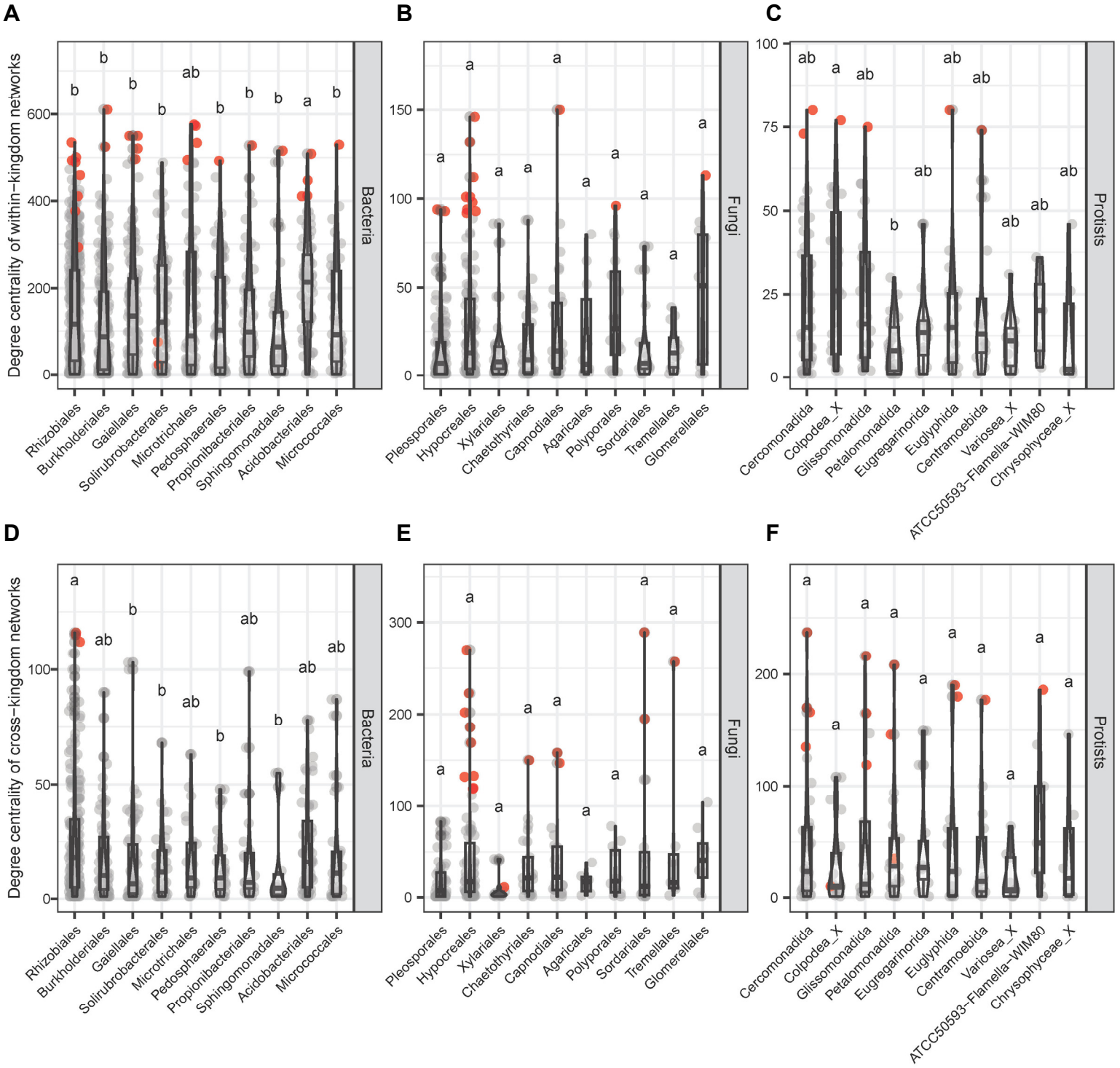

Extended Data Fig. 11. Taxonomic order-specific degree centrality in intrakingdom and interkingdom networks reveals bacterial domination and protist-fungal keystone roles in interkingdom network, related to Fig. 3

(**A–C**) Boxplots comparing degree centrality of intrakingdom networks: Bacteria: Boxplots (interquartile range) with red points marking hub ASVs show Acidobacteriales exhibiting highest degree centrality (vertical axis). Statistically surpasses Rhizobiales ($P = 0.009$), Burkholderiales ($P = 7.02 \times 10^{-5}$), and other bacterial orders. Letter annotations (a, b) denote Tukey HSD groupings ($P < 0.05$). Fungi/Protists: Consistently low centrality values across orders (grey points: non-hub ASVs).

(**D–F**) Boxplots comparing degree centrality of interkingdom networks: Protists & Fungi: Cercomonadida (protists) and Hypocreales (fungi) dominate centrality (red points: hubs). Bacteria: Limited hub roles (red points) despite high ASV count. Grey points indicate non-hub ASVs. Letter annotations (a, b, c) mark statistical groupings.

Extended Data Fig. 12

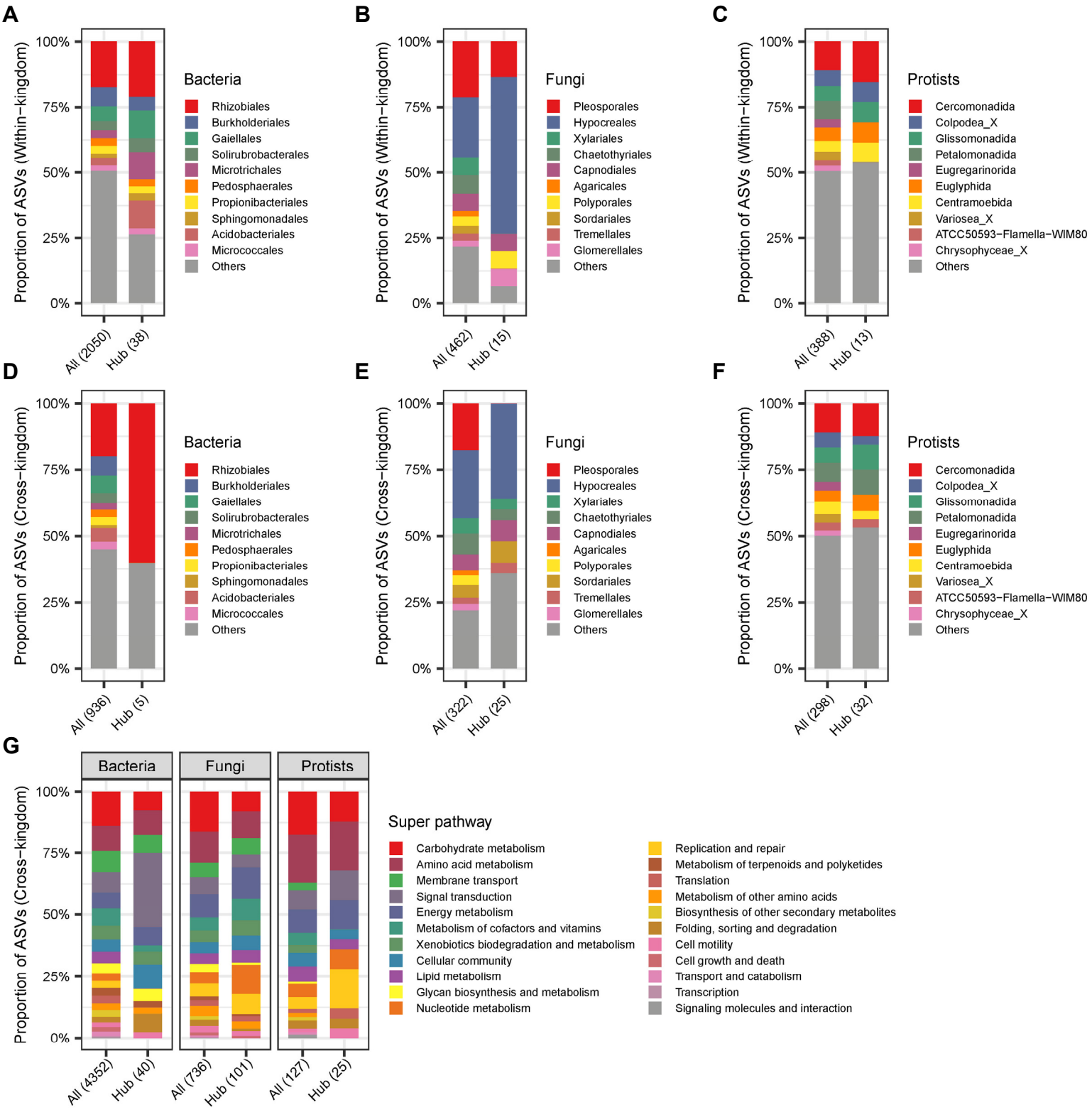

Extended Data Fig. 12. Taxonomic hub enrichment and functional specialization in rhizosphere networks, related to Fig. 3

(**A–C**) Intrakingdom hub enrichment: Comparative bar plots (All ASVs vs. Hub ASVs) reveal order-level specialization: Bacteria: Rhizobiales, Gaiellales, Micrococcales, and Acidobacteriales dominate hubs; Fungi: Hypocreales (Ascomycota), Polyporales (Basidiomycota), and Glomerellales enriched; Protists: Cercomonadida (Cercozoa), Euglyphida, and Centramoebida enriched. (**D–F**) Interkingdom hub enrichment: Bacteria: Rhizobiales dominate hubs Fungi: Hypocreales, Capnodiales, Sordariales, and Tremellales prevalent; Protists: Cercomonadida, Glissomonadida, Petalomonadida, and Euglyphida as keystones. (**G**) Functional specialization of hub KOs: Bacteria & Protists: Enriched signal transduction (e.g., *cheA*, *rcsB*). Fungi: Broad metabolic specialization: Energy metabolism, Cofactor/vitamin synthesis, Nucleotide metabolism, and DNA replication/repair.

Extended Data Fig. 13

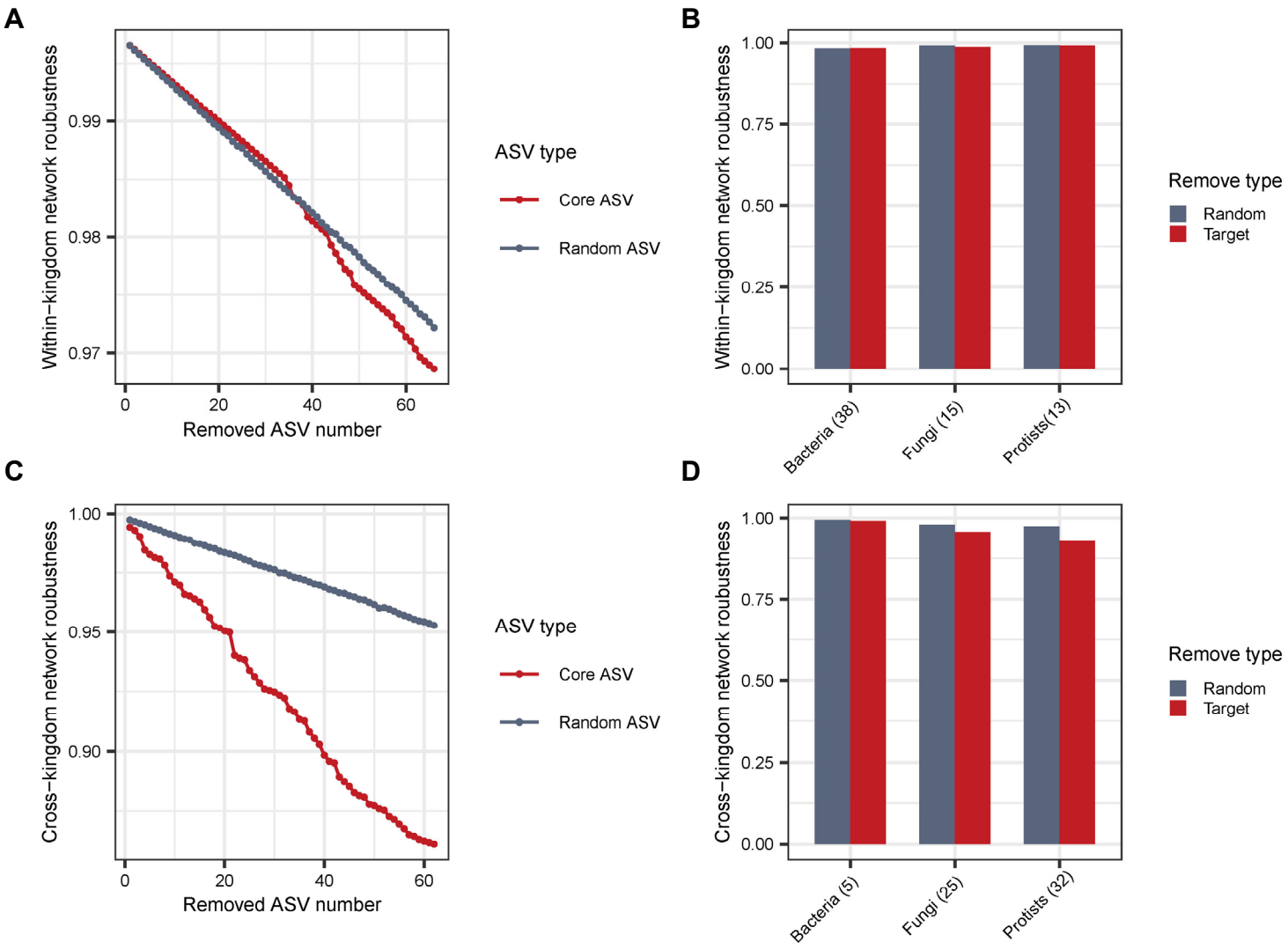

Extended Data Fig. 13. Network robustness analysis confirms protists and fungi as critical keystones, related to Fig. 3

(**A**) Decline in intrakingdom network robustness following progressive removal of core ASVs (red) vs. random ASVs (blue).

(**B**) Post-removal robustness: Intrakingdom networks showed minimal disruption when all hubs were removed.

(**C, D**) Parallel analyses for interkingdom networks: (C) Steeper decline when removing core ASVs (red line, slope = –0.0015) vs. random (blue, slope = –0.0003). (D) Removal of fungal/protistan hubs disproportionately reduced robustness (fungi: Δ = –0.02; protists: Δ = –0.04) vs. bacterial hubs (Δ = –0.0035).

Extended Data Fig. 14

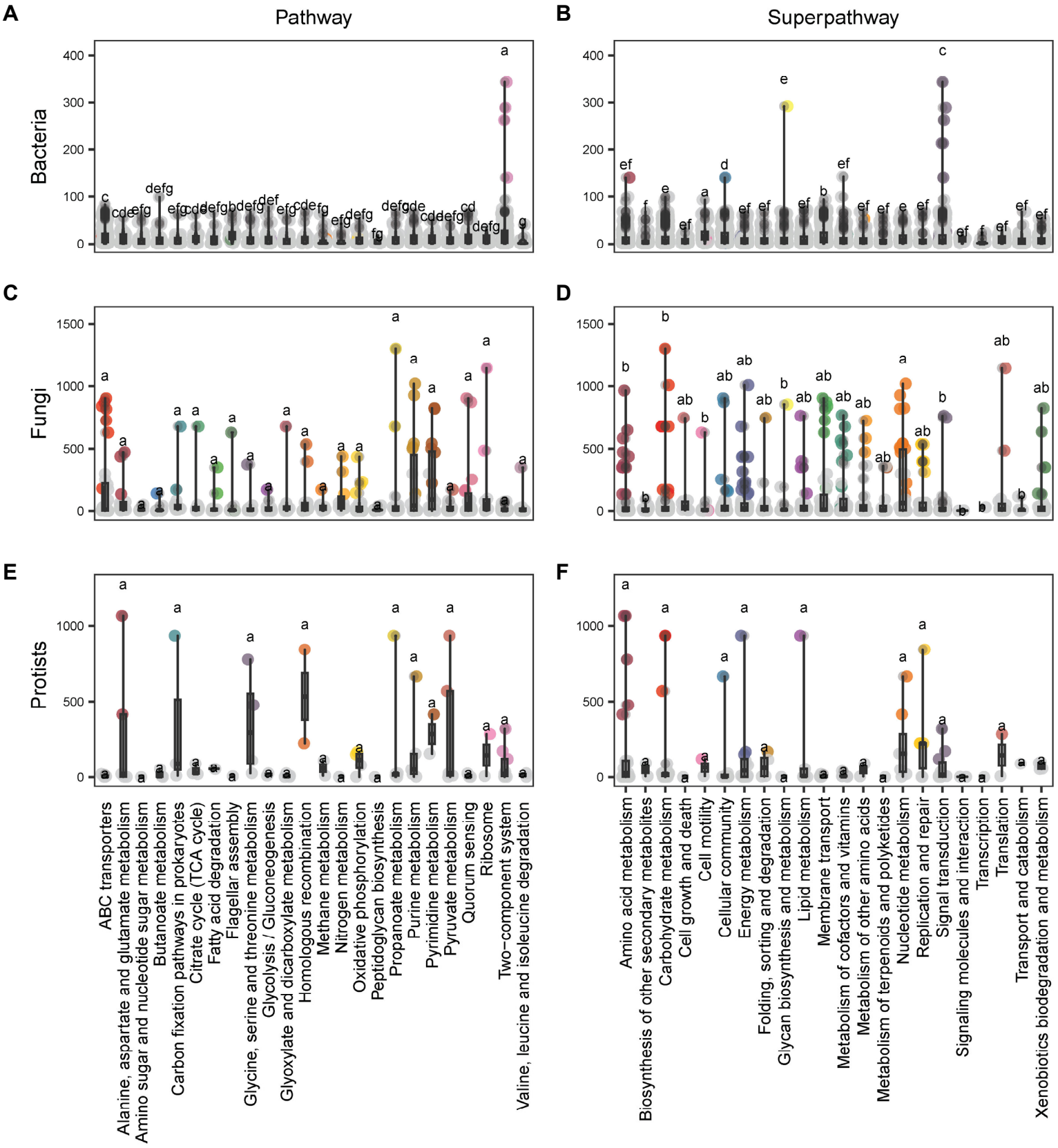

Extended Data Fig. 14. Kingdom-specific functional hub ko enrichment reveals convergent core metabolism and divergent specialization, related to Fig. 3.

(**A–B**) Distribution of bacterial functional hub KOs across KEGG pathway (A) and superpathway (B) levels. Bar plots show dominance in two-component systems (pathway level) and signal transduction (superpathway level).

(**C–D**) Distribution of fungal functional hub KOs across KEGG pathway (C) and superpathway (D) levels. Hub KOs are distributed across broad functional categories.

(**E–F**) Distribution of protistan functional hub KOs across KEGG pathway (E) and superpathway (F) levels. Letters (a-g) denote significant statistical hierarchies ($P < 0.05$, ANOVA with Tukey's post-hoc test; a = highest, g = lowest).

Extended Data Fig. 15

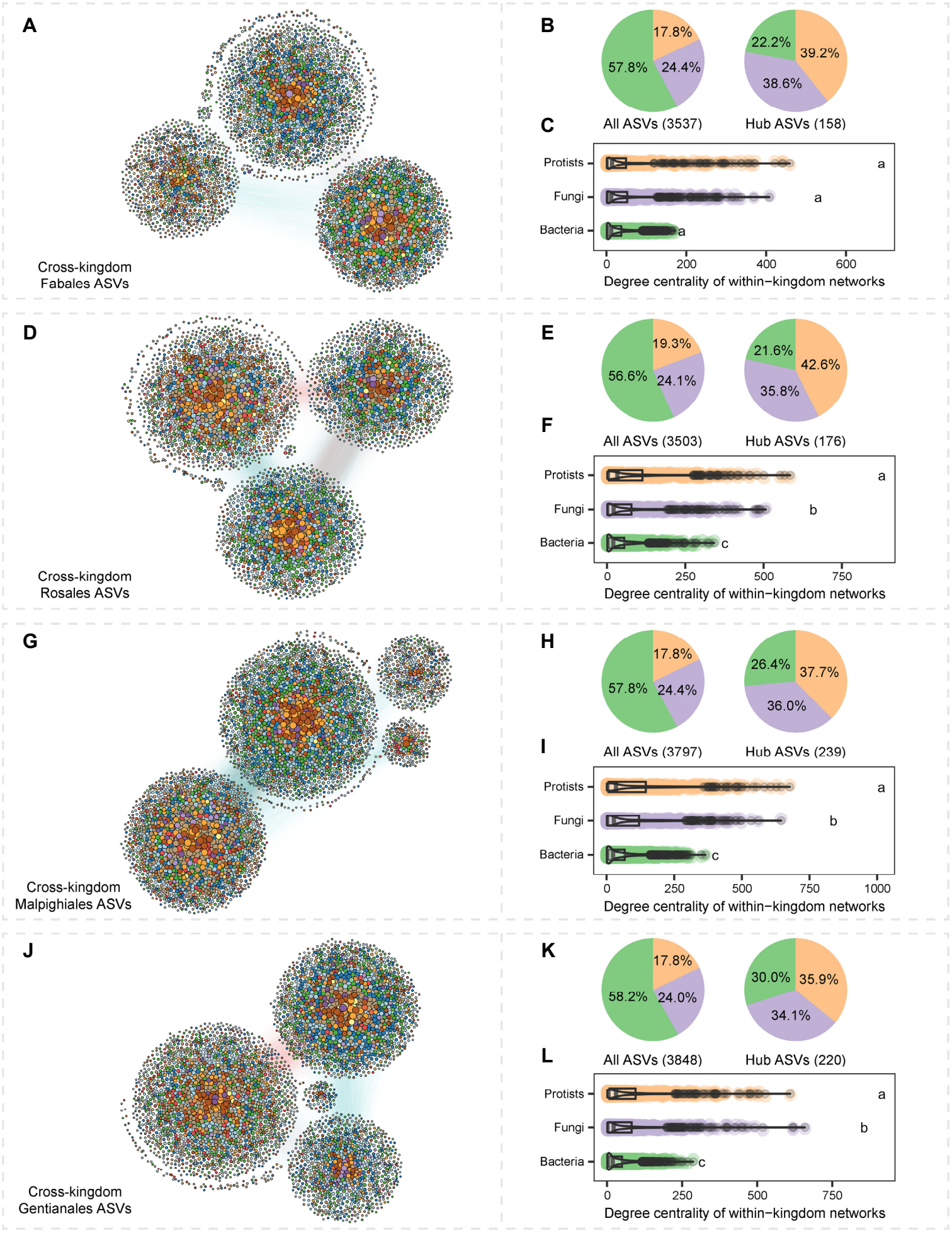

Extended Data Fig. 15. Conserved fungal and protistan hub dominance across plant lineages validates interkingdom keystone taxa, related to Fig. 4D-F.

(A,D,G,J) Interkingdom co-abundance networks with bacteria, fungi, and protists for Fabales, Gentianales, Malpighiales and Rosales, respectively. Node size reflects degree centrality. Hub ASVs concentrate in fungal/protistan clusters.

(B,E,H,K) Hub ASV distribution. Pie charts compare taxonomic distribution of total ASVs vs. hub ASVs. Fungi and protists consistently dominate hubs (all >70% combined).

(C,F,I,L) Kingdom centrality comparisons. Degree centrality boxplots confirm significantly higher fungal/protistan connectivity than bacteria ($P < 0.001$). Letters a/b/c denote Tukey HSD groupings ($P < 0.05$).

Extended Data Fig. 16

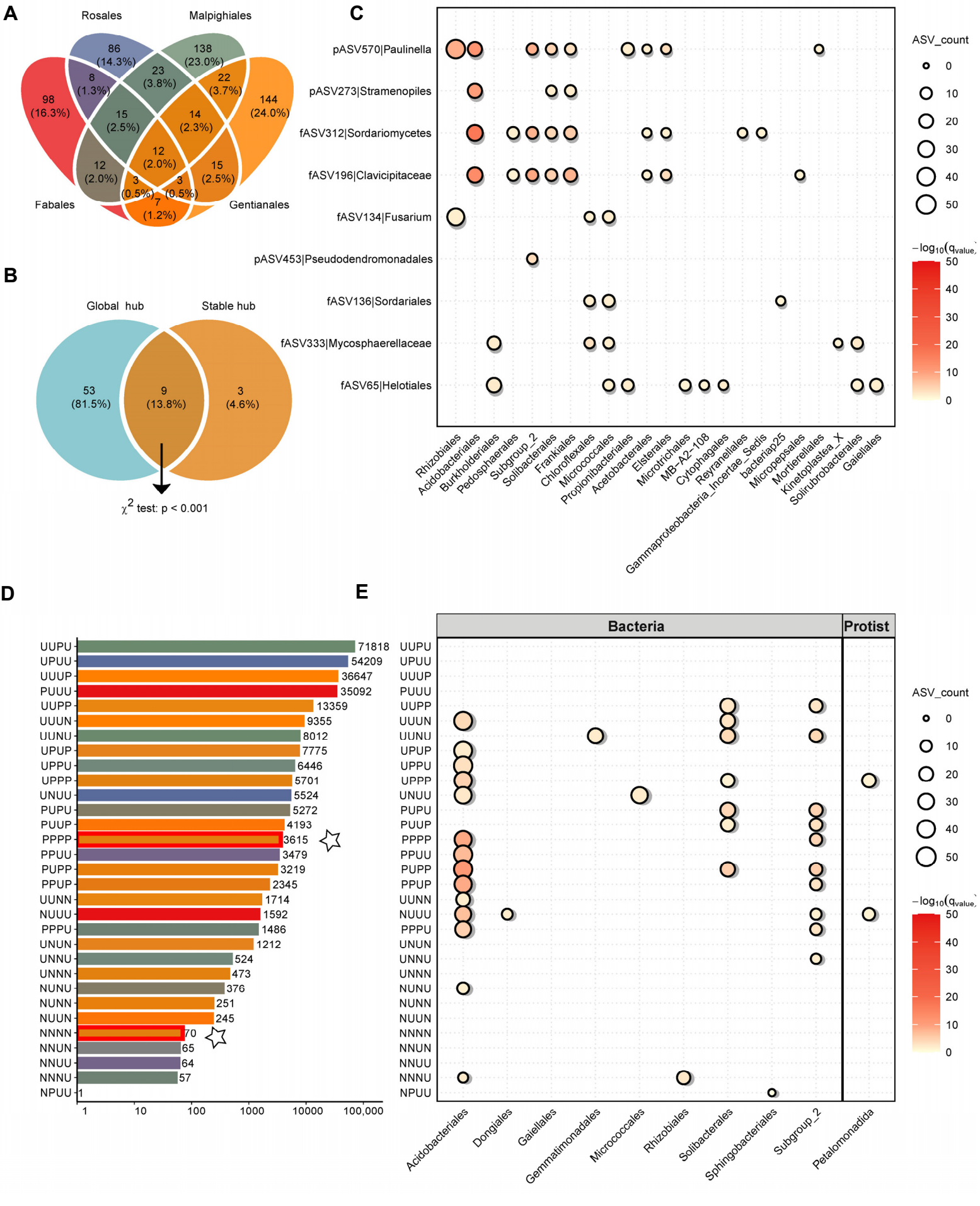

Extended Data Fig. 16. Conserved hubs and stable interactions reveal hierarchical functional modularity in rhizosphere microbiomes, related to Fig. 4

(**A**) Plant order-specific core ASV overlap: Venn diagram quantifies shared fungal/protistan hubs across Fabales, Rosales, Malpighiales, and Gentianales. Malpighiales hosts the highest unique hubs, while 12 ASVs (e.g., pASV570|*Paulinella*) are conserved globally ($P < 0.001$).

(B) Venn diagram showing the overlap among hub ASVs in global network (from Extended Data Fig. 3D) and conserved across four plant orders. *P* values refer to enrichment results using chi-square test.

(**C**) Taxonomic association of hub ASVs: Bubble plot shows bacterial order preferences of hub ASVs. Color indicates statistical significance ($-\log_{10}(\text{Padj})$); size indicates ASV enrichment ratio.

(**D**) Stable correlation persistence: Bar chart classifies interkingdom ASV correlation types. Cross-order conserved edges (PPPP: 3,615; NNNN: 70) reflecting resilient ecological relationships.

(**E**) Microbial enrichment for stable correlations. Bubble plot showing enriched microbial orders in stable ASV correlations. Color intensity reflects $-\log_{10}(\text{Padj})$.

Extended Data Fig. 17

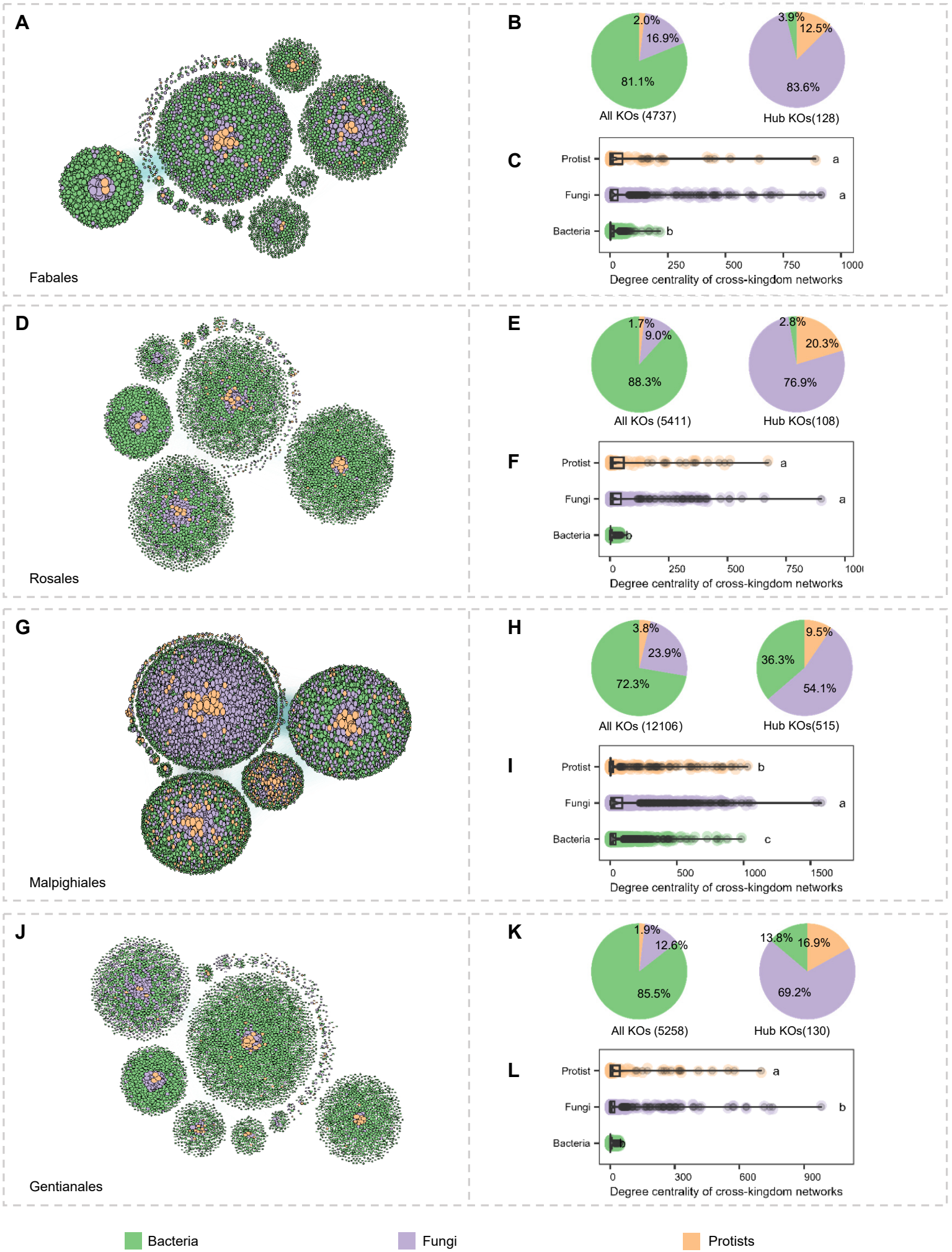

Extended Data Fig. 17. Metagenomic functional network robustness across plant lineages confirms kingdom-specific keystone roles, related to Fig. 3G-I.

(A,D,G,J) Interkingdom KO co-abundance networks with bacteria, fungi, and protists for Fabales, Gentianales, Malpighiales and Rosales, respectively. Node size reflects degree centrality. Hub KOs concentrate in fungal/protistan clusters.

(B,E,H,K) Hub KO distribution. Pie charts compare taxonomic distribution of total KOs vs. hub KOs. Fungi and protists consistently dominate hubs (all >64% combined).

(C,F,I,L) Kingdom centrality comparisons. Degree centrality boxplots confirm significantly higher fungal/protistan connectivity than bacteria ($P < 0.001$). Letters a/b/c denote Tukey HSD groupings ($P < 0.05$).

Extended Data Fig. 18

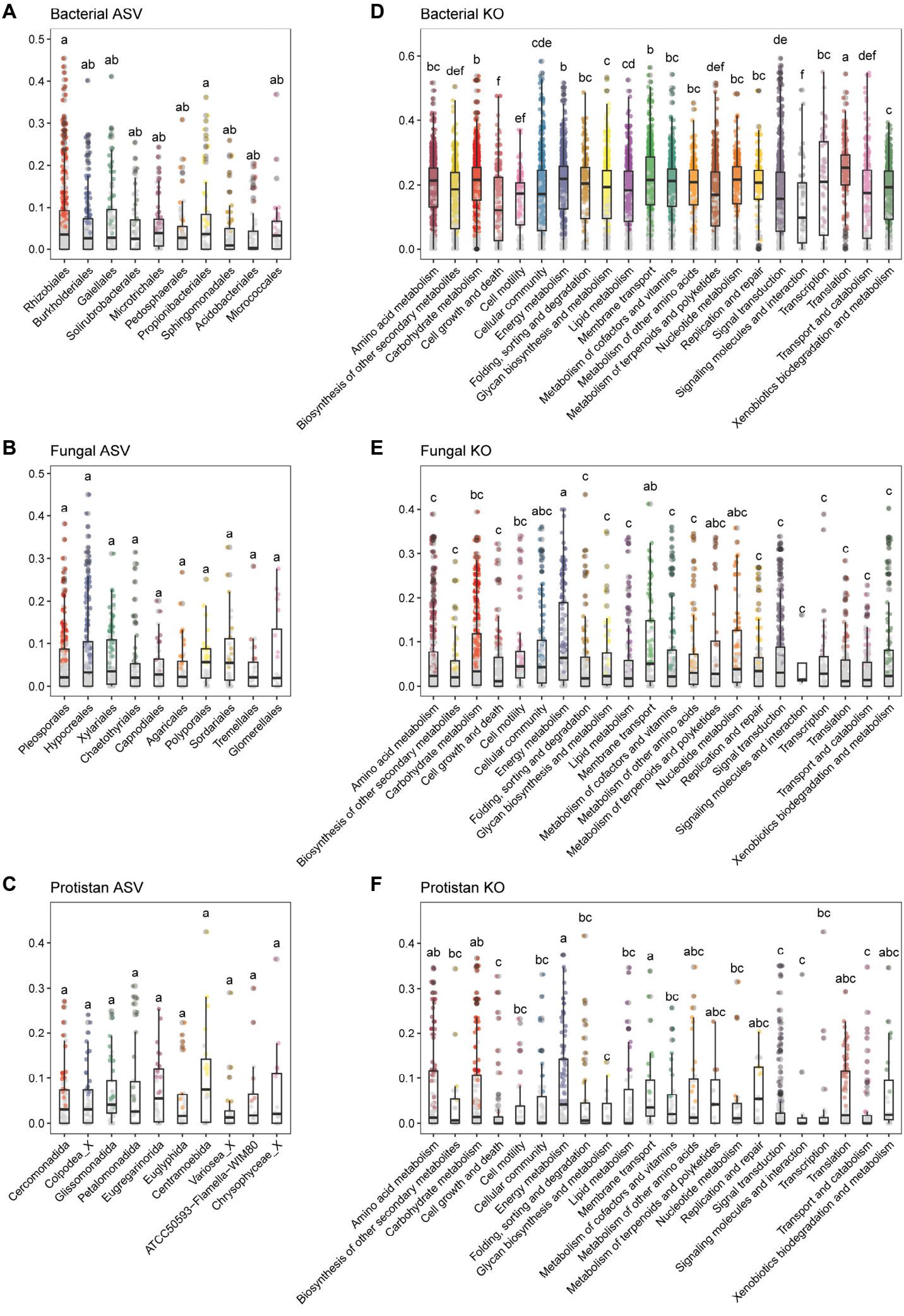

Extended Data Fig. 18. Domain-specific signatures of taxonomic and functional phylogenetic conservation in plant-microbe coevolution, related to Fig. 5A-C

(**A-C**) Taxonomic enrichment of phylogenetically conserved ASVs: (A) Bacteria: Concentrated in symbiotic orders Rhizobiales (48 ASVs; 10 symbiotic Rhizobium-allied genera) and Burkholderiales (21 ASVs). (B) Fungi: Dominated by Pleosporales (37 ASVs) and Hypocreales (48 ASVs). (C) Protists: No order-level enrichment (uniform distribution).

(**D-F**) Functional superpathway enrichment of phylogenetically conserved KOs in bacteria (D), fungi (E) and protists (F): Phylogenetically conserved KOs exhibit strong signals ($\lambda > 0.5$) in: Cellular community (e.g., biofilm/quorum sensing), Membrane transport (ABC transporters, secretion) and Signal transduction (two-component systems). Colored points: (Pagel's λ test, q-value < 0.05); Grey points: (Pagel's λ test, q-value ≥ 0.05).

Extended Data Fig. 19

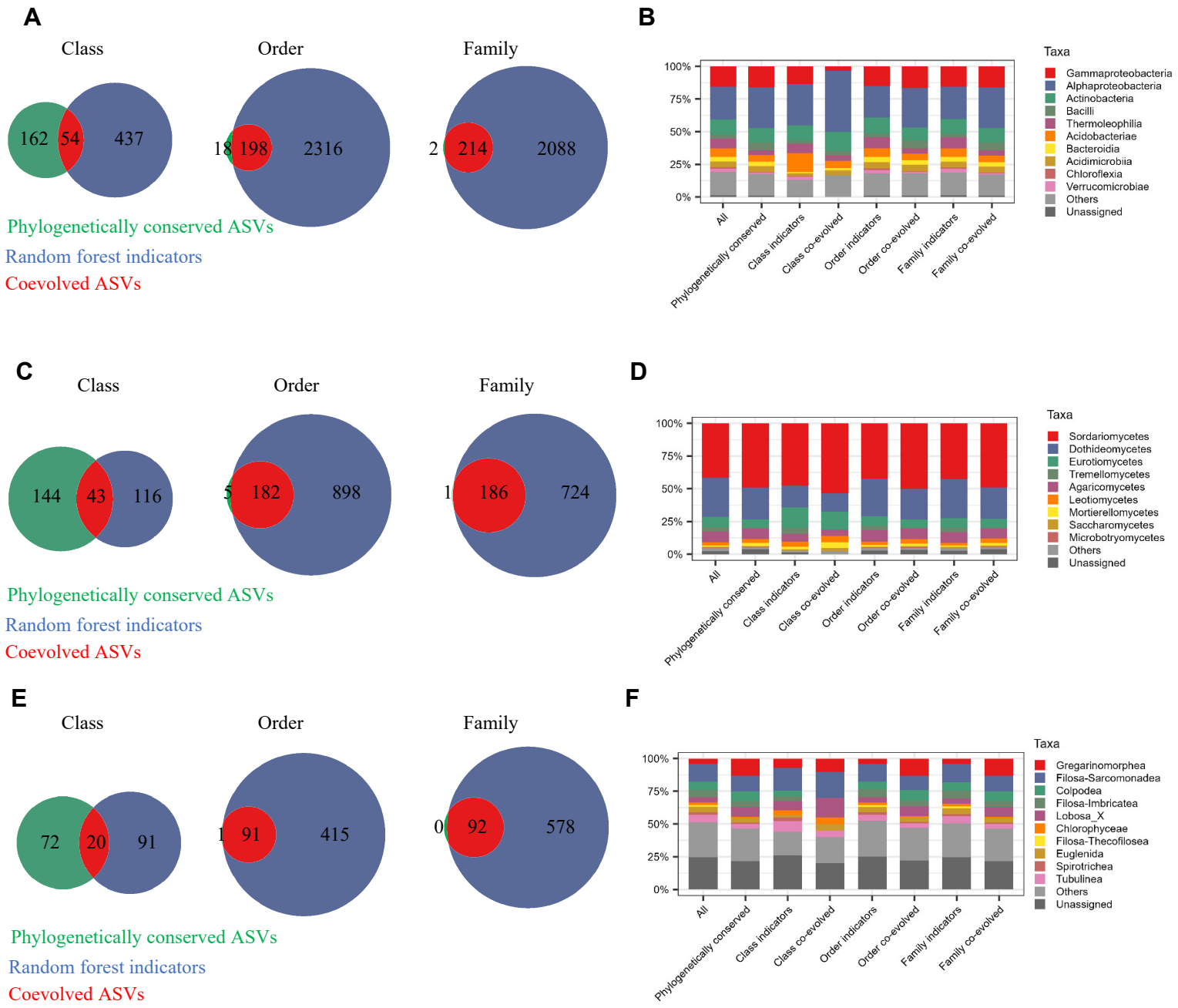

Extended Data Fig. 19. Phylogenetically conserved and co-evolved asvs reveal domain-specific evolutionary dynamics in rhizosphere microbiomes, related to Fig. 5A-C.

(**A–B**) Bacterial co-evolution: (A) Venn diagram showing intersections: phylogenetically conserved ASVs (green), RF indicators (blue), and co-evolved ASVs (red). Co-evolved ASVs included 54 class-, 198 order-, and 214 family-level lineages. (B) Taxonomic distribution: Compared to core ASVs and RF indicators, co-evolved ASVs were enriched in Alphaproteobacteria and Bacilli, but depleted in Thermoleophilia and Acidobacteriae.

(**C–D**) Fungal co-evolution: (C) Venn diagram showing intersections: phylogenetically conserved ASVs (green), RF indicators (blue), and co-evolved ASVs (red). Co-evolved ASVs included 43 class-, 182 order-, and 186 family-level lineages. (D) Taxonomic distribution: Compared to core ASVs and RF indicators, co-evolved ASVs were enriched in Sordariomycetes and Leotiomycetes, but depleted in Dothideomycetes.

(**E–F**) Protistan co-evolution: (E) Venn diagram showing intersections: phylogenetically conserved ASVs (green), RF indicators (blue), and co-evolved ASVs (red). Co-evolved ASVs included 20 class-, 91 order-, and 92 family-level lineages. (F) Taxonomic distribution: Compared to core ASVs and RF indicators, co-evolved ASVs were enriched in Gregarinomorphea and Colpodea, but depleted in Filosa.

Extended Data Fig. 20

Extended Data Fig. 20. KEGG Enrichment reveals functional phylogenetic conservation overwhelmingly outpaces taxonomic signals in rhizosphere microbiomes, related to Fig. 5D-F.

Heatmap dot plots show KEGG pathway enrichment for: Left panels (Core genes): Bacterial, fungal, protistan core KOs. Right panels (Phylogenetically Conserved Genes, PCGs): Bacterial, fungal, protistan KOs with significant plant co-evolution (Pagel's λ; FDR < 0.05). Dot properties: Color intensity (red) = $-\log_2$(qvalue); dot size = KO counts.

Extended Data Fig. 21

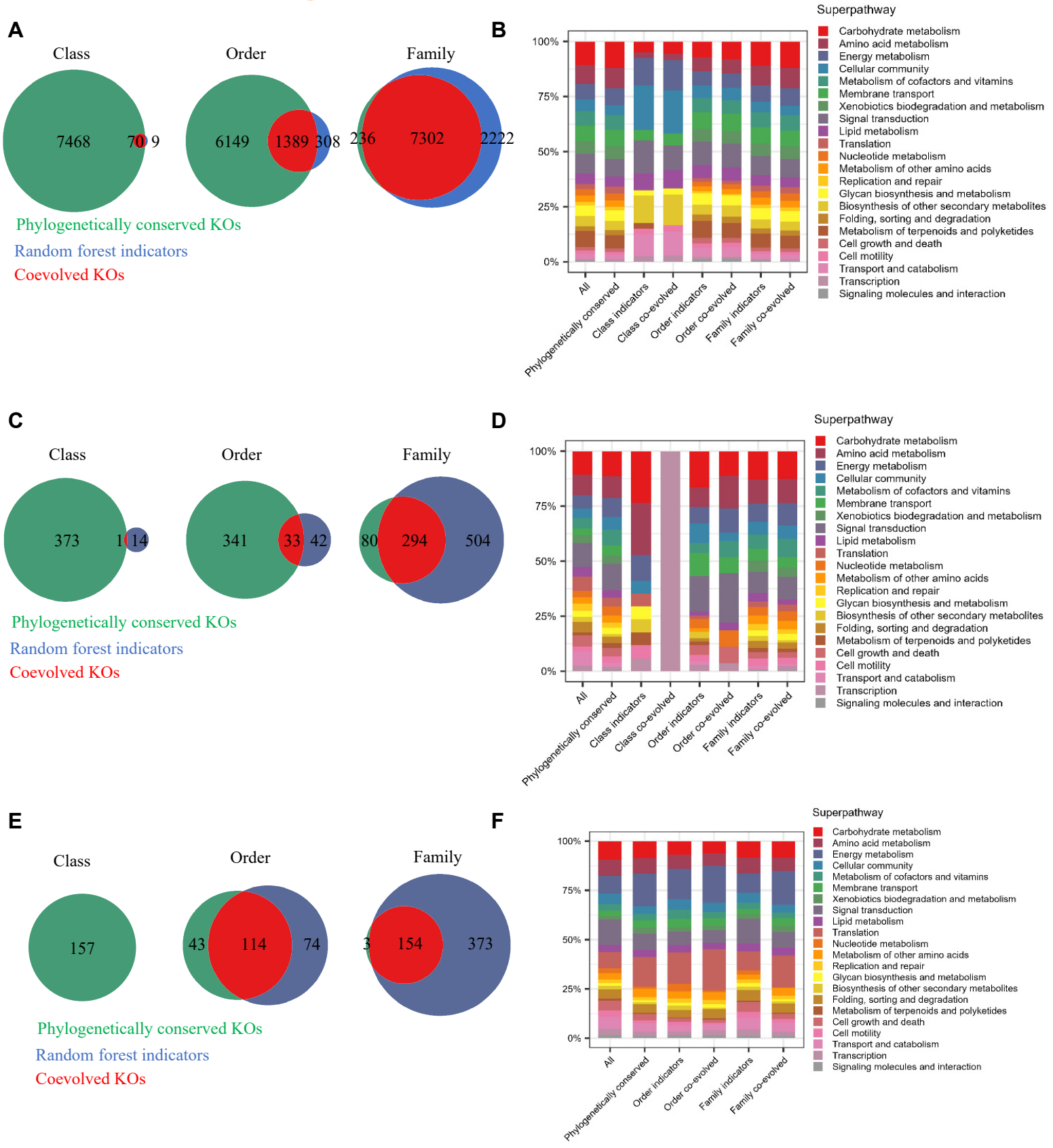

Extended Data Fig. 21. Phylogenetically conserved and co-evolved kos reveal bacteria dominate functional coevolution with plants, related to Fig. 5D-F.

(**A–B**) Bacterial function co-evolution: (A) Venn diagram showing intersections: phylogenetically conserved KOs (green), RF indicators (blue), and co-evolved KOs (red). (B) KEGG super-pathway distribution of core KOs, RF indicators, and co-evolved KOs.

(**C–D**) Fungal function co-evolution: (C) Venn diagram showing intersections: phylogenetically conserved KOs (green), RF indicators (blue), and co-evolved KOs (red). (D) KEGG super-pathway distribution of core KOs, RF indicators, and co-evolved KOs.

(**E–F**) Protistan function co-evolution: (E) Venn diagram showing intersections: phylogenetically conserved KOs (green), RF indicators (blue), and co-evolved KOs (red). (F) KEGG super-pathway distribution of core KOs, RF indicators, and co-evolved KOs. In plant class level, no RF indicators and co-evolved KOs were identified.

Extended Data Fig. 22

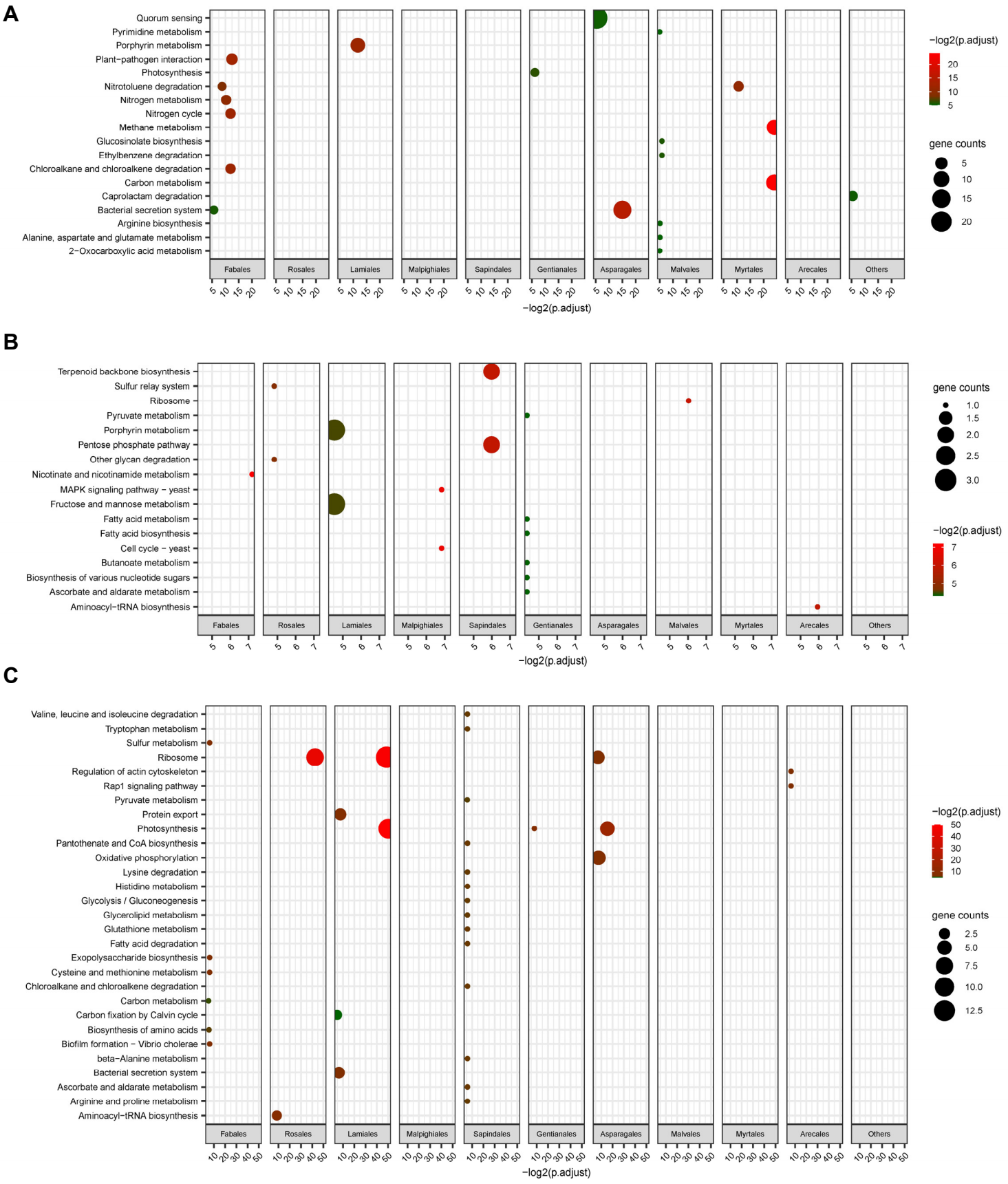

Extended Data Fig. 22. Order-specific functional signatures of plant-microbe coevolution reveal kingdom-divergent strategies, related to Fig. 5D-F.

(**A**) Bacterial KO enrichment across plant orders: Bubble plots showing KEGG pathway enrichment for coevolved bacterial KOs highlighting exclusive enrichment in Fabales.

(**B**) Fungal KO enrichment across plant orders. Bubble plots showing KEGG pathway enrichment for coevolved fungal KOs.

(**C**) Protistan KO enrichment across plant orders: Bubble plots showing KEGG pathway enrichment for coevolved protistan KOs, highlighting exclusive enrichment in Asparagales/Lamiales:

Extended Data Fig. 23

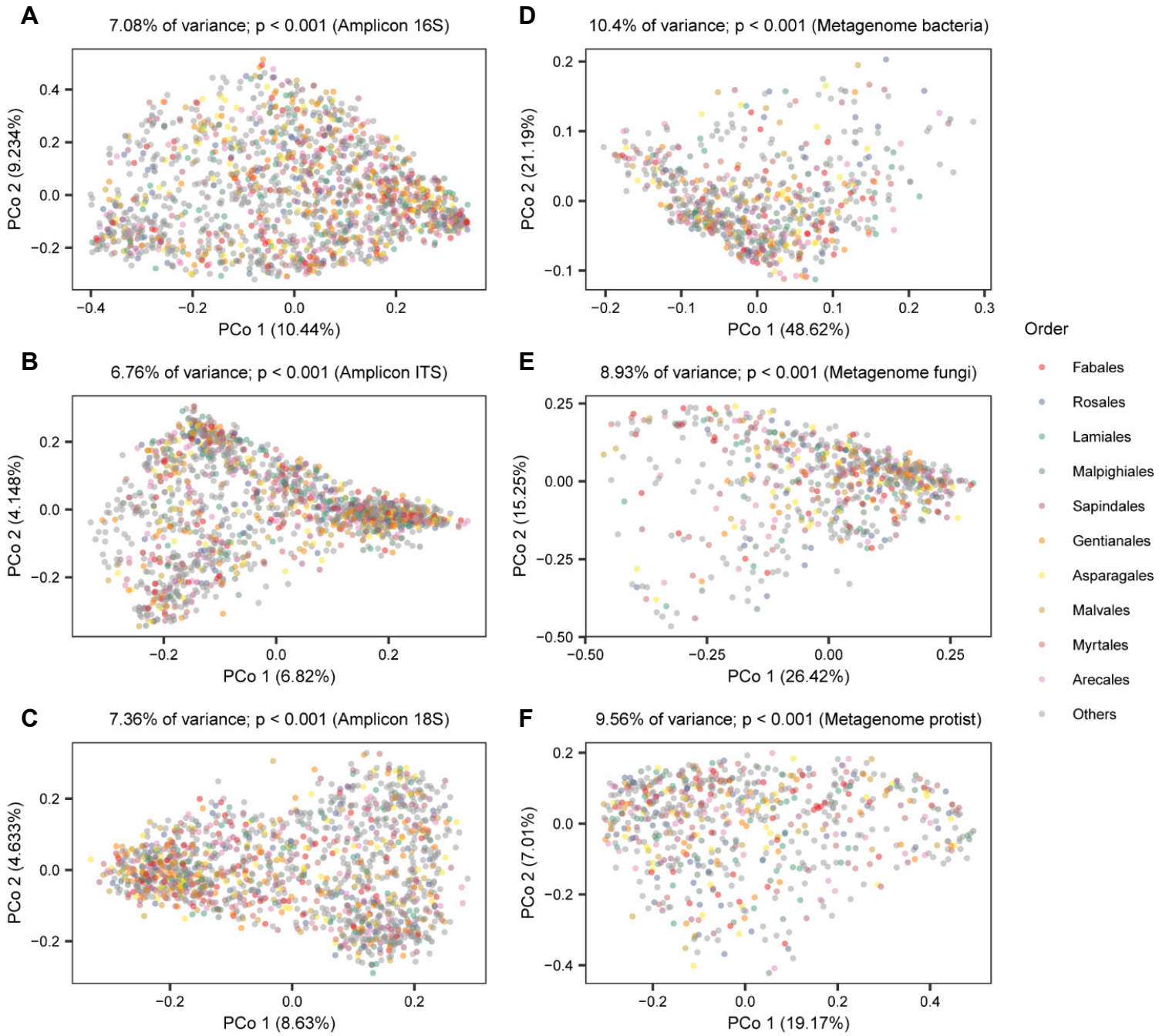

Extended Data Fig. 23. PCoA reveals host phylogeny-driven microbial community differentiation across taxonomic and functional domains, related to Supplementary Information Table 8A

(**A–C**) Principal Coordinate Analyses (PCoA) of Bray-Curtis dissimilarities for bacterial 16S rRNA gene (A), fungal ITS (B), and protistan 18S rRNA gene (C).

(**D–F**) Principal Coordinate Analyses (PCoA) of Bray-Curtis dissimilarities for metagenomic sequences assigned to bacteria (D), fungi (E), and protists (F).

Extended Data Fig. 24

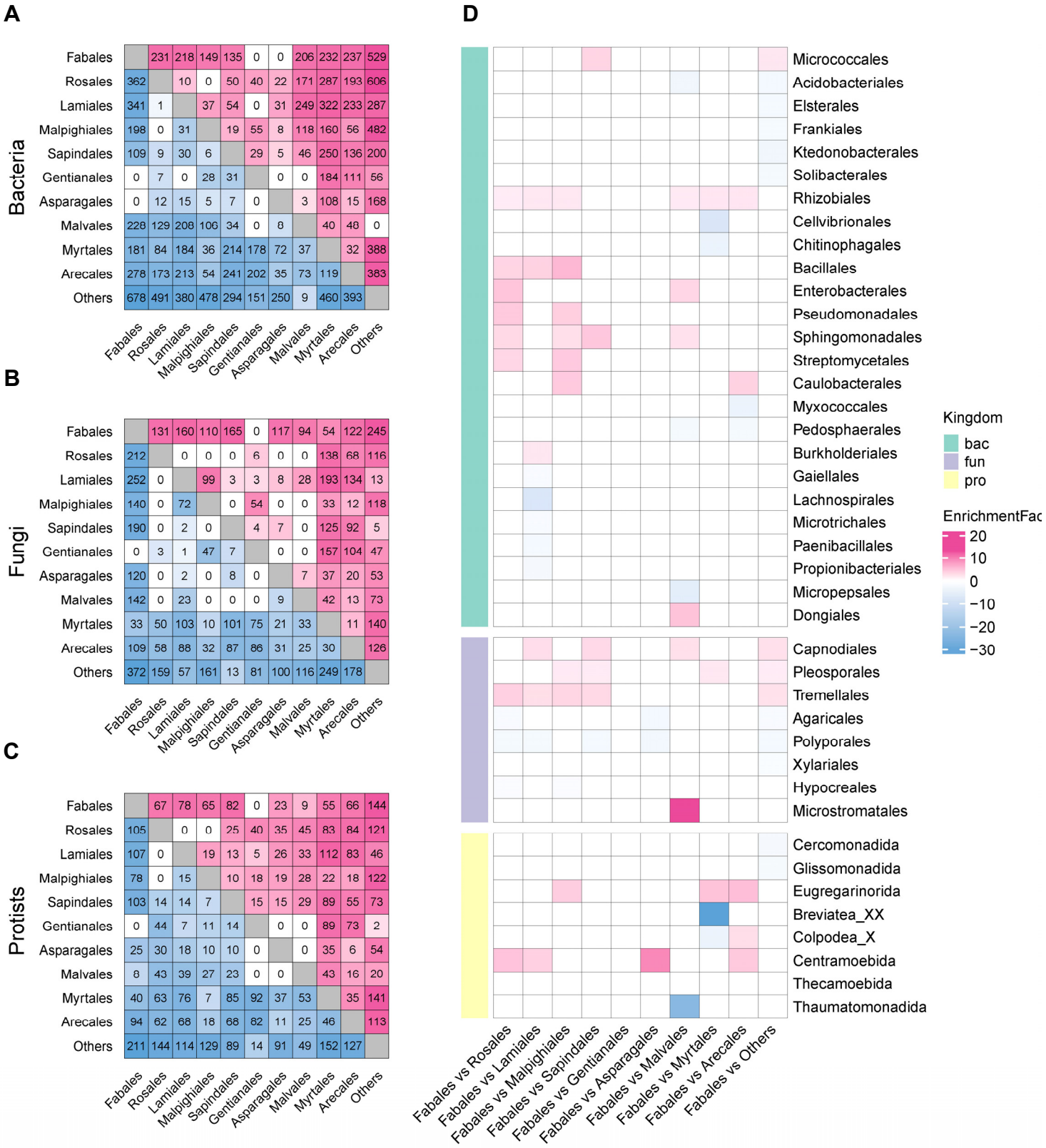

Extended Data Fig. 24. Host-specific microbial selection defines the Fabales rhizosphere as a distinct niche with unique enrichment-depletion dynamics, related to Supplementary Information Table 8B

(**A-C**) Heatmaps of differential ASV abundances for bacteria, fungi, and protists across 10 plant orders (columns: target order; rows: comparison group). Pink cells (upper right triangle): number of ASVs significantly increased in target rhizosphere (e.g., +231 bacterial ASVs in Fabales vs. Rosales). Blue cells (lower left triangle): number of ASVs significantly decreased in target rhizosphere (e.g., -362 bacterial ASVs in Fabales vs. Rosales).

(**D**) Taxonomic enrichment of ASVs significantly increased/decreased in Fabales rhizosphere (Fabales vs. other orders).

Pink cells: Taxa enriched among ASVs increased in Fabales. Blue cells: Taxa enriched among ASVs decreased in Fabales.

Extended Data Fig. 25

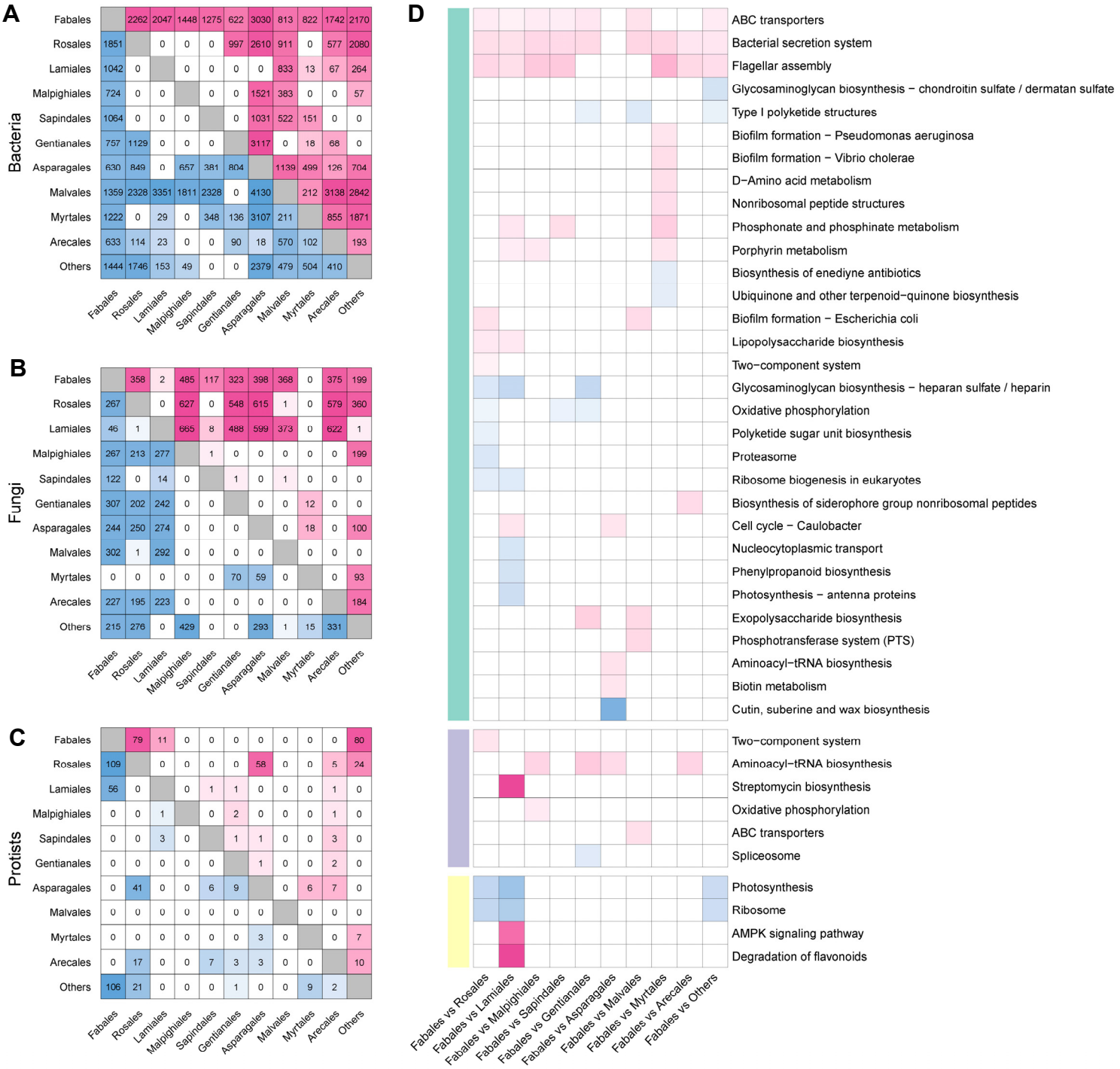

Extended Data Fig. 25. Fabales drives lineage-specific functional divergence in rhizosphere microbiomes, related to Supplementary Information Table 8C

(**A–C**) Differential KO abundance heatmaps for bacteria (A), fungi (B), and protists (C) across 10 plant orders. (columns: target order; rows: comparison group). Pink cells (upper right triangle): Number of KOs significantly increased in target rhizosphere (e.g., +2262 bacterial KOs in Fabales vs. Rosales). Blue cells (lower left triangle): Number of KOs significantly decreased in target rhizosphere (e.g., -1951 bacterial KOs in Fabales vs. Rosales).

(**D**) KEGG pathway enrichment of KOs significantly increased/decreased in Fabales rhizosphere (Fabales vs. other orders). Pink cells: KEGG pathway enriched among KOs increased in Fabales. Blue cells: KEGG pathway enriched among KOs decreased in Fabales.

Extended Data Fig. 26

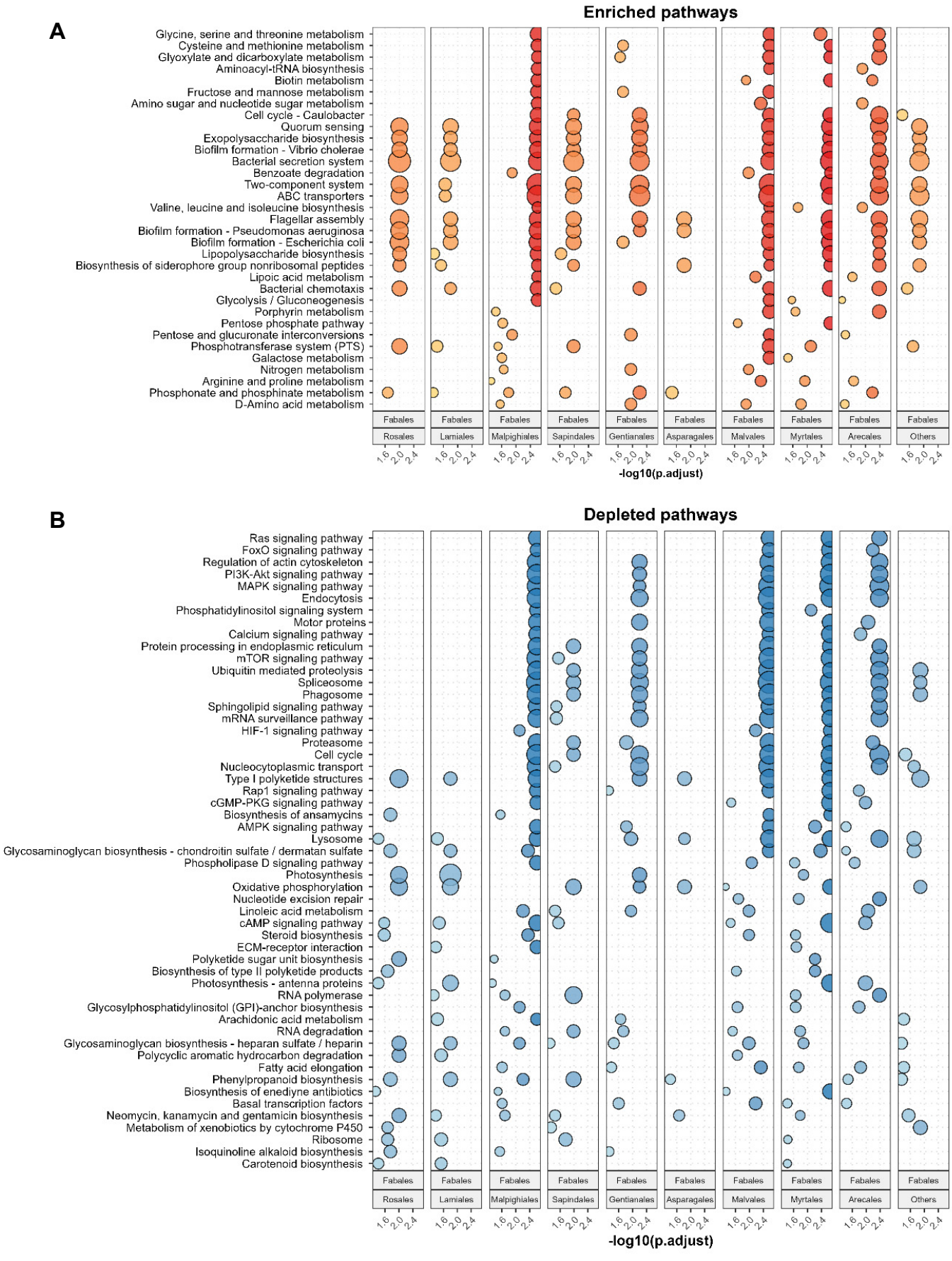

Extended Data Fig. 26. GRSA reveals Fabales rhizosphere functional trade-offs: Enhanced symbiotic metabolism at the expense of immune/detox pathways, related to Supplementary Information Table 8D

(**A**) Systemically enriched pathways in Fabales rhizospheres, including: microbial environmental sensing (e.g., bacterial secretion systems, two-component signaling), intercellular communication (e.g., quorum sensing, biofilm formation), and adaptive survival mechanisms (e.g., flagellar assembly, ABC transporters) .

(**B**) Systemically depleted pathways in Fabales rhizospheres, including host Immunity, chemical defense and detoxification.